AFCRC-TN-56-273

TURBULENT DIFFUSION OF MOMENTUM AND HEAT FROM A SMOOTH, PLANE BOUNDARY WITH ZERO PRESSURE GRADIENT

By

J.E. Cermak and A.C. Spengos

Department of Civil Engineering

FINAL REPORT - PART II

PRESENTATION OF DATA AND ANALYSIS

The research reported in this document has been sponsored by the Geophysics Research Directorate of the Air Force Cambridge Research Center, Air Research and Development Command, under Contract AF19(604)-421.

Colorado Agricultural and Mechanical College
Fort Collins, Colorado

December 1956

U18401 0590853

CER No. 56 JEC22

ABSTRACT

The research program conducted under Contract AF 19(604)-421 was a systematic experimental study to determine the effects of a lapse upon the characteristics of a turbulent boundary layer flow having a zero longitudinal pressure gradient. Lapse conditions were created by placing a 6- x 10-ft heated plate to form the floor of a wind tunnel test section 6- x 6-ft square and drawing air through the test section to create a turbulent boundary layer on the plate. Details of the wind tunnel arrangement and instrumentation to measure mean velocities and temperatures, intensities of velocity and temperature fluctuations, Reynolds stress and heat input to the plate are described in Final Report - Part I (11)[1].

Vertical distributions of mean velocities and temperatures for lapse conditions, intensity of velocity fluctuations and Reynolds shear stress for both neutral and lapse conditions at ambient velocities of 10, 17 and 35 fps together with heat transfer coefficients are given in Scientific Report No. 1 (9). Eddy viscosity distributions are presented in the same report for both neutral and lapse conditions at ambient velocities of 10, 17 and 35 fps.

An effort was made to determine the eddy conductivity ϵ_H[2]. This work is presented in Reference 10. As a result of measurements

[1] The first number of a pair of numbers in a parenthesis refers to the reference entry and the second number to the appropriate page.
[2] Symbols are defined under Symbols.

and analyses made during the course of this research, one can estimate that the ratio of eddy conductivity ϵ_H to eddy viscosity under lapse conditions ϵ_L is near unity.

In this report dimensional reasoning is used in an attempt to correlate various dependent parameters of the flow with the significant independent parameters. A brief study is made to determine the effects of a roughness trip or "turbulence stimulator" located upstream from the heated plate and to determine the state of development of the turbulent flow over the plate under neutral conditions. Comparisons are made, where possible, with similar data obtained in the atmospheric surface layer. The principal conclusions reached are as follows:

1. For neutral flow, the distribution of eddy viscosity ϵ_N is approximated by

$$\frac{\epsilon_N}{\nu} = 0.190 \left(\frac{U_*}{U_a} \right)^2 \left(R\, \delta_N^* \right)^{3/2}$$

for $2.5 < y/\delta_N^* < 5$. This result should be considered as applicable only when $1600 < R_{\delta_N^*} < 6400$.

2. Mean velocity profiles under lapse conditions in the wind tunnel show the same typical change of curvature as do mean velocity profiles for the atmospheric surface layer with a lapse. Only above a height over the smooth boundary at which the viscous forces become negligible does this similarity hold; therefore, if atmospheric surface layer similarity is to be improved, wind tunnel boundaries should be roughened.

3. Eddy viscosity under lapse conditions ϵ_L can be correlated with ϵ_N within the range of these studies through the expression

$$\frac{\epsilon_L - \epsilon_N}{\nu_0} = F \delta_N^{*\,-\frac{1}{4}} R_x \phi\left(\frac{y}{\delta_N^*}\right) = \left| Ri\, \delta_N^* \right|^{\frac{1}{8}} R_x \phi\left(\frac{y}{\delta_N^*}\right) .$$

4. The mean temperature distributions are similar when (y/δ_t^*) is used as a similarity parameter, provided $\delta_t \doteq \delta_L$.

CONTENTS

ACKNOWLEDGMENTS

The financial support of the Geophysics Research Directorate of the Air Force Cambridge Research Center, the early assistance of Mr. Benjamin Davidson and the stimulating relationship with Dr. Heinz Lettau, Contract Monitor, during the course of this research are gratefully acknowledged.

The writers are deeply indebted for the assistance of Mr. B. Chanda, Research Assistant, the editing of Mr. R. Shen, the computing of Mr. L. Fletcher, the drafting of Mr. J. Pope and the typing of Miss R. Sekora in the preparation of this report.

The administrative guidance and encouragement given by Prof. T. H. Evans, Dean of Engineering; Dr. D. F. Peterson, Jr., Head of the Department of Civil Engineering; and Dr. M. L. Albertson, Professor of Civil Engineering, have been very helpful during the performance of this study.

SYMBOLS

c_f	local drag coefficient -- $\frac{2\tau_o}{\rho U_a^2}$
c_p	specific heat of air at constant pressure
g	gravitational acceleration
k	Karman constant
ℓ	mixing length
n	exponent
r	one point velocity correlation coefficient for u and v
t	temperature fluctuation about T
t'	root-mean-square value of the local temperature fluctuation
u	instantaneous velocity fluctuation from U in the direction of x
$\overline{uv}$	Reynolds stress -- $\rho u'v'$
u'	root-mean-square value of the fluctuating component of the local velocity in the direction of x
v	instantaneous velocity fluctuation from V in the direction of y
v'	root-mean-square value of the fluctuating component of the local velocity in the direction of y
x	distance downstream from the beginning of the heated boundary
x_r	length of roughness trip
x'	distance downstream from the upstream edge of the roughness trip
y	distance measured vertically from the surface of the heated boundary
y_r	height of roughness elements in roughness trip

$F_{\delta_N^*}$ Froude number -- $\dfrac{U_a}{\sqrt{g(\Delta\rho/\rho_o)\,\delta_N^*}}$

$G_{\delta_N^*}$ Grashof number -- $g\dfrac{\Delta T}{T_a}\dfrac{\delta_N^{*3}}{\nu_o^2}$

K thermal conductivity of air

K_t thermal diffusivity of air -- $\dfrac{k}{c_p\rho}$

Pr Prandtl number -- $\dfrac{\nu}{K_t}$

R_x Reynolds number -- $\dfrac{U_a x}{\nu_o}$

$R_{\delta_N^*}$ Reynolds number -- $\dfrac{U_a\,\delta_N^*}{\nu_o}$

$Ri_{\delta_N^*}$ Richardson number -- $\dfrac{g\dfrac{\Delta T}{\delta_N^*}}{(T_a)\,(U_a/\delta_N^*)^2}$

T local mean temperature

T_o mean temperature at the surface of the heated boundary from x = 0 to measuring station

T' root-mean-square value of temperature fluctuations about T

ΔT $(T_a - T_o)$

U x-component of the local mean velocity

U_* mean shear velocity on the surface of the heated boundary -- $\sqrt{\tau_o/\rho}$

U_a mean ambient velocity

V y-component of the local mean velocity

δ thickness of the momentum boundary layer (value of y for $U = 0.99\ U_a$)

δ_t thickness of the thermal boundary layer (value of y for $T = T_o - 0.99\Delta T$)

δ^* displacement thickness -- $\int_o^\infty \left(1 - \frac{\rho}{\rho_o}\frac{U}{U_o}\right)dy$

δ_t^* temperature thickness -- $\int_o^\infty (1 - \theta)dT$

ϵ eddy viscosity

ϵ_H eddy conductivity

θ dimensionless mean temperature -- $\frac{(T - T_o)}{(T_a - T_o)}$

μ dynamic viscosity of air

ν kinematic viscosity of air

ρ density of air

$\Delta\rho$ $(\rho_a - \rho_o)$

τ shearing stress in the direction of x in a plane perpendicular to the y-coordinate

Subscripts

L indicates quantity for lapse conditions

N indicates quantity for neutral conditions

a refers to values for ambient conditions

o refers to values for $y = 0$ at temperature T_o

DATA SYMBOLS

Symbol		U_a (approx.)	x	T_a	T_a °F	ΔT °F
Neutral	Lapse	fps	ft	Neutral	Lapse	Lapse
○	○	6	0.29	50	65	110
⊖	⊖	6	0.96	50	68	108
⊖	⊖	6	3.29	50	69	100
●	●	6	9.30	53	72	94
○	○	10	0.29	59	70	118
⊖	⊖	10	0.96	59	74	112
⊖	⊖	10	3.29	59	75	111
●	●	10	9.30	59	72	107
○	○	17	0.29	55	50	93
⊖	⊖	17	0.96	54	51	90
⊖	⊖	17	3.29	52	52	85
●	●	17	9.30	48	50	82
○	○	35	0.29	44	64	62
⊖	⊖	35	0.96	49	67	61
⊖	⊖	35	3.29	52	63	60
●	●	35	9.30	54	60	58

I. INTRODUCTION

Turbulent shear flows of fluids with their associated diffusion phenomena are of considerable theoretical interest and great practical importance as well as frustration to those who encounter them in various applications. The apparent complexity of such flow fields requires those who treat practical problems of heat transfer, evaporation, transport of immiscible masses, and flow resistance to rely upon the results of experimental investigations. Most of the experimental data collected have been of a form that appears in the semi-empirical mixing length and similarity theories of turbulence and have been analyzed on the basis of dimensional arguments. While this approach has given immediate practical results, a mechanism of turbulent shear flows consistent with the equations of motion is still not known.

With the development of hot-wire anemometers and the formulation of a statistical theory of homogeneous turbulence, emphasis is now being placed upon determination of the structure of shear flows by measuring velocity fluctuation spectra and correlations. Even though the statistical theory of homogeneous turbulence has met with some success in describing energy dissipation at high frequencies in accordance with Kolmogoroff's hypothesis, the anisotropic low frequency disturbances which affect the diffusion phenomena are not well understood. The present state of these developments is summarized by Townsend (13).

When the quantity being diffused interacts with a turbulent shear flow to alter the dynamic characteristics of the flow from those which would exist were the diffusing quantity not present, a more

complex state is encountered than has been considered in the previously mentioned theories. In order to gain some knowledge of such flows, experimental studies must be conducted. As in this research, several other investigators have considered the interaction of heat upon a turbulent boundary layer formed over a heated flat plate. Johnson (5) has made measurements of many of the statistical correlations arising in the statistical theory of turbulence for a boundary layer flow over a smooth, flat, heated plate. A low temperature difference of 60°F and a moderately large ambient velocity of 25 fps were purposely chosen to make the interaction effects negligible. However, an increase in the vertical velocity fluctuation intensity and the Reynolds stress near the heated plate may have been attributable to buoyancy forces created by the heating. Batchelor (1) refers to measurements of velocity and temperature fluctuation intensities made by Nicholl in a turbulent boundary layer formed over a smooth, flat, heated plate. At an ambient air speed of 7.9 fps and an air-plate temperature difference of 175°F he found the longitudinal velocity fluctuation intensity to be increased by 1.7 times that for a zero temperature difference. In addition, a high correlation coefficient of about -0.65 for the longitudinal velocity fluctuations and the temperature fluctuations shows a large degree of interaction between the diffusion of heat and the flow characteristics. A well known effect of heat transfer from a horizontal flat plate to a laminar boundary layer of air forming over it is a decrease in the Reynolds number of transition to turbulent flow. The work of Liepmann and Fila (7) shows that the effects of viscosity variation due to heating from below is sufficient to cause the observed result.

The experimental study herein described was designed to yield information useful in determining the effects of heat transfer to a turbulent boundary layer. Development of the boundary layer took place over a smooth and flat, horizontal, heated plate forming the floor of a wind tunnel test section with zero longitudinal pressure gradient. A roughness trip was used upstream from the heated plate to produce a thickened turbulent boundary layer. Figs. 1 and 2 describe the wind tunnel and the experimental arrangement schematically. Primarily, the effects of an unstable density stratification upon the vertical distribution of mean velocity, eddy viscosity, mixing length, and velocity fluctuation intensities were sought. To attain this goal, vertical distributions of mean velocity, mean temperature, velocity and temperature fluctuation intensities, and one point correlation coefficients for horizontal and vertical velocity fluctuations were measured at four stations for both neutral and lapse conditions. During the creation of a lapse, electrical power supplied to heat the plate was measured thus enabling determination of heat transfer coefficients. The equipment and techniques used to obtain the foregoing data are described in Part I of this report -- Spengos and Cermak (11). Data were obtained for the four ambient air speeds of 6, 10, 17, and 35 fps for ambient air-plate surface temperature differences of zero for all speeds and of 110°F, 115°F, 85°F, and 60°F for each of the four speeds respectively. The basic data are recorded in Tables I and II. A preliminary reporting of the data together with eddy viscosities, drag coefficients and heat transfer coefficients for all ambient speeds except 6 fps was

made in Scientific Report No. 1 -- Spengos (9). Comparable data for the 6 fps ambient velocity consisting of vertical profiles of Reynolds shear stress and horizontal and vertical velocity fluctuation intensities are presented in Fig. 3. An attempt to infer the magnitude of the thermal eddy conductivity has been made. This work appears in the paper of Spengos and Cermak (10).

The primary objective, as previously stated, was to determine the effects of buoyancy forces caused by heating from below upon characteristics of the turbulent boundary layer. The secondary objective was to ascertain the similarities and dissimilarities, where possible, of a wind tunnel boundary layer flow and flow in the atmospheric surface layer with a lapse. An effort is made to achieve the primary objective in the sequel by first analyzing the neutral and lapse cases separately by dimensional reasoning. Comparisons of neutral flows and flows with a lapse are then made in the spirit of Prandtl's and Boussinesq's formulations -- comparisons of mean velocities, mixing lengths and eddy viscosities. The statistical quantities of horizontal and vertical velocity fluctuation intensities and Reynolds shear stress are compared through an isotropy ratio and the correlation coefficient. The ratio of mixing velocity (intensity of vertical velocity fluctuation) to mixing length which plays an important role in the model of turbulence for a nonadiabatic atmosphere according to Lettau (4:68) is examined for effects due to heating. Finally, the temperature fluctuation intensity data are presented. The secondary objective is sought by comparing the mean velocity profiles for flow in the atmospheric surface layer with those obtained in the wind tunnel and by comparison of

the isotropy ratio and the correlation coefficient for the two environments.

II. DIMENSIONAL ANALYSIS

Dimensional arguments are used in the following paragraphs to arrive at appropriate dimensionless groupings of the important variables for the cases of neutral and lapse conditions. For the neutral state, the mean velocity U and the eddy viscosity ϵ_N are considered as separate dependent variables. Dependent variables for flow with a lapse are chosen as the mean velocity U in one instance and the eddy viscosity ϵ_L in another. Other variables which may be chosen as dependent quantities are the correlation coefficient r, the isotropy ratio u'/v', the mixing length ℓ, the ratio v'/ℓ, the mean temperature Θ, and the intensity of temperature fluctuations T'. These are briefly considered.

Neutral Flow Field

Mean Velocity Distribution

Because of the uncertainty that full development of a turbulent boundary layer will occur downstream from a roughness trip for values of x'/x_r little larger than unity and for relatively small velocities, a systematic examination of vertical mean velocity distribution dependency is essential. To meet this need, a dimensional analysis is useful.

For the prescribed flow geometry, the mean velocity U will be a function of several independent variables

$$U = U\,(U_a\,,\ L\,,\ \rho\,,\ \mu\,,\ x_r\,,\ y_r\,,\ y)\ . \qquad (1)$$

Upon using the displacement thickness δ_N^* as the characteristic length L , Eq 1 may be transformed into the following dimensionless expression:

$$\frac{U}{U_a} = U_1 \left(R\,\delta_N^* , \frac{x_r}{\delta_N^*} , \frac{y_r}{\delta_N^*} , \frac{y}{\delta_N^*} \right) . \qquad (2)$$

The displacement thickness δ_N^* is used as a reference length because it may be determined accurately. The mean velocity U_a is used for a reference velocity rather than U_* because of uncertainties in evaluation of the latter. For sufficiently large $R\,\delta_N^*$, U/U_a should become a function of y/δ_N^* alone if the roughness trip characteristics have negligible effect upon the flow structure. Clauser (2) has shown that a strictly universal distribution of velocity is never attained but is only approached within the practical limits of measurement accuracy. However, large variations from universality will be interpreted as due to effects created by the roughness trip or due to incomplete development of the turbulence structure.

Eddy Viscosity Distribution

Introduction of the concept of an eddy viscosity ϵ_N is a very useful artifice provided some knowledge of how ϵ_N varies with the flow conditions and boundary distance is at hand. The variable ϵ_N may be considered a function of the same variables introduced for U in Eq 1. If one assumes a negligible effect of the roughness trip on the flow structure, the eddy viscosity may be generally expressed as

$$\epsilon_N = \epsilon_N \left(U_a , \delta_N^* , \rho , \mu , y \right) . \qquad (3)$$

This leads to

$$\frac{\epsilon_N}{\nu} = \epsilon_{N_1}\left(R_{\delta_N^*}, \frac{y}{\delta_N^*}\right) \quad , \tag{4}$$

in a non-dimensional formulation. Thus, the Boussinesq number ϵ_N/ν becomes a function of the Reynolds number $R_{\delta_N^*}$ and the dimensionless coordinate y/δ_N^*.

Some knowledge of the form of Eq 4 can be obtained by writing

$$\rho\epsilon_N \frac{dU}{dy} = \tau_{turb} \tag{5}$$

$$= \tau_o\left[1 - f\left(\frac{y}{\delta_N^*}\right)\right] \tag{6}$$

if the turbulent shear stress is assumed to be a universal function of $\frac{y}{\delta_N^*}$. By taking $U_*^2 = \tau_o/\rho$ and assuming

$$\frac{U}{U_a} = g(\zeta) \quad , \tag{7}$$

where $\zeta = y/\delta_N^*$, Eq 6 may be rearranged to give

$$\frac{\epsilon_N}{\nu} = \left(\frac{U_*}{U_a}\right)^2 \left(\frac{U_a \delta_N^*}{\nu}\right) \left(\frac{dg}{d\zeta}\right)^{-1} \left[1 - f(\zeta)\right] \quad . \tag{8}$$

The dependence of ϵ_N/ν upon $R_{\delta_N^*}$ and ζ can be seen better if Eq 8 is written as

$$\frac{\epsilon_N}{\nu} = \left(\frac{U_*}{U_a}\right)^2 R_{\delta_N^*} G(\zeta) = \frac{c_f}{2} R_{\delta_N^*} G(\zeta) \quad . \tag{9}$$

Eq 9 is now in the form of Eq 4 since c_f is some function of $R_{\delta_N^*}$.

In Chapter III, an attempt is made to determine the form of G which is consistent with the measurements made in this study.

In Scientific Report No. 1(9:14) an attempt was made to compare the experimentally determined values of ϵ_N with those computed through assumption of a logarithmic velocity distribution and those computed through the use of Reichardt's modification of the logarithmic velocity distribution. In calculating ϵ_N when dU/dy was obtained from the two different logarithmic distributions, the assumption was made that $U_* = -\sqrt{\overline{uv}}$. Since this assumption is unrealistic, a comparison of ϵ_N will be made which does not involve the foregoing assumption. For the logarithmic velocity distribution one has instead of Eq 9 in Reference 9:14,

$$\frac{\epsilon_N}{U_a \delta_N} = - \frac{k y \overline{uv}}{U_a \delta_N U_*} \quad . \tag{10}$$

In place of Eq 10 in Reference 9:15, the Reichardt modification gives

$$\frac{\epsilon_N}{U_a \delta_N} = - \frac{k \overline{vu}}{U_a U_* \left[\frac{1}{y/\delta_N} - \frac{1}{(2 - y/\delta_N)} + \frac{7.5(1 - y/\delta_N)^{1/2}}{1 + 5(1 - y/\delta_N)^{3/2}} \right]} \quad . \tag{11}$$

Eqs 10 and 11 are used in Chapter III for calculating $\epsilon_N/(U_a \delta_N)$ and the results are compared with $\epsilon_N/(U_a \delta_N)$ in which dU/dy has been obtained graphically from the measured velocity distribution.

Flow Field with a Lapse

Mean Velocity and Temperature Distributions

Measurements of mean velocity and velocity fluctuation intensities have shown that for the range of temperature differences and

ambient velocities studied, thermal effects are predominant over any residual effects of the roughness trip, therefore, roughness trip characteristics will be omitted from the following arguments. Consideration of the dependency of U leads to the following formulation:

$$U = U(\rho_o, \mu_o, c_{p_o}, k_o, g, \Delta T, T_a, U_a, \delta_N^*, x, y) \quad . \tag{12}$$

In dimensionless form, Eq 12 may be rewritten

$$\frac{U}{U_a} = U_1\left(\frac{U_a \delta_N^*}{\nu_o}, \frac{k_o}{\rho_o c_{p_o} U_a \delta_N^*}, \frac{\Delta T}{T_a}, g\frac{\Delta T}{T_a}\frac{\delta_N^{*3}}{\nu_o^2}, \frac{x}{\delta_N^*}, \frac{y}{\delta_N^*}\right) . \tag{13}$$

The second dimensionless parameter in Eq 13 may be written as a product of $\left(\frac{k_o}{\rho_o c_{p_o} \nu_o}\right)\left(\frac{\nu_o}{U_a \delta_N^*}\right)$ which represents a product of the reciprocals of the Prandtl number and a Reynolds number. The Prandtl number is essentially constant over the range of temperature considered in this research; hence, the second parameter may be neglected. By the use of the perfect gas law, $\Delta T/T_a$ may be expressed as $-\Delta\rho/\rho_o$; thus, expressing the effect of density stratification upon inertia forces of the flow. This parameter may be combined with a parameter $U_a^2/(g\,\delta_N^*)$ arising in the dimensional analysis to give a Froude number $F_{\delta_N^*} = U_a/(g\frac{\Delta\rho}{\rho_o}\delta_N^*)^{1/2}$. Such a number represents the ratio of inertia forces to buoyancy forces when squared and can easily be shown to be identical to $Ri_{\delta_N^*}^{-1/2}$. The parameter $\left(g\frac{\Delta T}{T_a}\right)\frac{\delta_N^{*3}}{\nu_o^2}$ is a form of Grashof number and characterizes the ratio of buoyancy forces to viscous resistive forces. An interesting formulation of this parameter is obtained by forming the product

$$\frac{g\ \Delta T/\delta_N^*}{T_a\ U_a^2/\delta_N^{*2}}\left(\frac{U_a \delta_N^*}{\nu_o}\right)^2 \quad .$$

Hence, the Grashof number $G_{\delta_N^*}$ is equivalent to a bulk Richardson number $Ri_{\delta_N^*}$ multiplied by the square of a Reynolds number $R_{\delta_N^*}$. Eq 13 may be slightly rearranged to show the dependency of U/U_a on the six dimensionless parameters as follows:

$$\frac{U}{U_a} = U_2 \left(R_x , R_{\delta_N^*} , G_{\delta_N^*} , F_{\delta_N^*} , \frac{y}{\delta_N^*}\right) . \tag{14}$$

When considering the mean temperature distribution, it is more significant to use δ_t^* in place of x. This modification leads to the following general form for Θ :

$$\Theta = \Theta \left(R_{\delta_t^*} , R_{\delta_N^*} , G_{\delta_N^*} , F_{\delta_N^*} , \frac{y}{\delta_t^*}\right) . \tag{15}$$

Eddy Viscosity Distribution

The eddy viscosity for flow with a lapse ϵ_L will be a function of the independent variables included in Eq 12. In dimensionless form, an expression for the Boussinesq number becomes

$$\frac{\epsilon_L}{\nu_o} = \epsilon_L \left(R_x , R_{\delta_N^*} , G_{\delta_N^*} , F_{\delta_N^*}, \frac{y}{\delta_N^*}\right) . \tag{16}$$

Since the effect of allapse upon the eddy viscosity is sought, it appears advantageous to consider the difference $(\epsilon_L - \epsilon_N)/\nu_o$. Considering that the difference indicated is due to the thermal conditions alone, one may write if the assumption is made that the effect of $R_{\delta_N^*}$ is additive in Eq 16

$$\frac{\epsilon_L - \epsilon_N}{\nu_o} = \Delta\epsilon \left(R_x , G_{\delta_N^*} , F_{\delta_N^*} , \frac{y}{\delta_N^*}\right) . \tag{17}$$

The parameter $R_{\delta_N^*}$ does not appear explicitly in Eq 17 since ϵ_N/ν_o is a function of $R_{\delta_N^*}$ and replaces it under the additive assumption. For purposes of correlating the data, the function in Eq 17 may be postulated to be of the form

$$\Delta\epsilon\,(R_x,\ G_{\delta_N^*},\ F_{\delta_N^*},\ \frac{y}{\delta_N^*}) = (R_x)^{n_1}\,(G_{\delta_N^*})^{n_2}\,(F_{\delta_N^*})^{n_3}\,\phi\left(\frac{y}{\delta_N^*}\right) . \quad (18)$$

Parameters for Other Dependent Flow Quantities

A complete investigation of the effect of a lapse upon dependent variables other than U and ϵ would lead to sets of independent parameters as given in Eq 14. Several dependent quantities which have appeared in turbulent flow theory capable of being evaluated from the measurements made during this research are as follows:

a. Correlation coefficient $r = \overline{uv}/u'v'$,

b. Isotropy ratio u'/v' ,

c. Mixing length $\ell = \sqrt{\overline{uv}}\left(\frac{dU}{dy}\right)^{-1}$,

d. Mixing velocity - mixing length ratio v'/ℓ ,

e. Temperature fluctuation intensity T' .

The correlation coefficient r is a statistic which gives some information on the local flow structure. If the velocity fluctuations are random, $r = 0$ and $r = \pm 1$ if the flow has a definite form, e.g. a vortex with axis fixed in space. In determining the departure of the local flow conditions from isotropy, the isotropy ratio is useful. A necessary condition for isotropy is that $u'/v' = 1$. This condition for a turbulent boundary layer in the wind tunnel is

approached only when $y \gtrsim \delta$. The mixing length ℓ was first introduced by Prandtl -- Schlichting (8:383) -- and the assumption of a magnitude proportional to wall distance was the first used. The ratio of mixing velocity to mixing length v'/ℓ is used by Lettau (4:68) in relating ϵ_N to ϵ_L . There the assumption made is that $(v'/\ell)_N = (v'/\ell)_L$.

The temperature boundary layer thickness δ_t may be used as a reference length. If such a reference length is used to correlate the temperature fluctuation intensities, there results a form for $T'/\Delta T$ given by

$$\frac{T'}{\Delta T} = T' \left(R_{\delta_t} , R_{\delta_N^*} , G_{\delta_N^*} , F_{\delta_N^*} , \frac{y}{\delta_t}\right) . \qquad (19)$$

In the following chapter, data for the foregoing dependent quantities will be given and discussed.

III. PRESENTATION OF DATA AND DISCUSSION

Mean velocity distribution data for the neutral flows are examined in an effort to detect any major effects resulting from the use of a roughness trip to thicken the turbulent boundary layer. The vertical distributions of ϵ_N are presented and the several sets of data are correlated through the use of significant dimensionless groups. The experimentally determined distributions of ϵ_N are compared with those obtained through the use of both the logarithmic velocity distribution and Reichardt's modification of the logarithmic velocity distribution to calculate the velocity gradient.

For flows with a lapse, mean velocity profiles are compared with those for the neutral case to detect variations in profile curvatures similar to those observed in the atmospheric surface layer under lapse conditions. The vertical distributions of mean temperature are examined for similarity. Special attention is given to comparing the values of ϵ_N and ϵ_L and to determining the dimensionless parameters which primarily affect their difference. Qualitative comparisons are made for vertical distributions of r, $-u'/v'$, ℓ/δ^*_N, and v'/ℓ under neutral and lapse conditions. Finally, vertical distributions of $T'/\Delta T$ are presented.

Neutral Flow Field

Vertical Distribution of Mean Velocity

The vertical distributions of mean velocity for neutral flow are examined in an effort to establish the flow conditions under which

the studies with unstable density variation took place. The following two questions should be answered:

1. Is the flow structure appreciably affected by the roughness trip other than through moving the apparent origin of the turbulent boundary layer upstream?
2. Is the flow equivalent to that of fully developed turbulence, or is the turbulence structure still developing?

The velocity profiles for each ambient velocity which are presented in Figs. 4, 5, 6 and 7 and the composite graph of Fig. 8 indicate that the general variation of mean velocity with y/δ^*_N in the "outer" region of the boundary layer is essentially the same as that found by Klebanoff and Diehl (6) for distances of over 3 ft from the downstream edge of their roughness trip. Fig. 4 shows two velocity profiles from the measurements of Klebanoff and Diehl for a fully developed turbulent boundary layer. They appear to be in good agreement with the present data throughout the boundary layer for $U_a = 35$ fps . The detailed measurements of Klebanoff and Diehl showed no significant variation of turbulence structure after the flow had developed such mean velocity profiles from that which existed for a naturally developed turbulent boundary layer. The roughness elements used in the present study have values of y_r about three times those used by Klebanoff and Diehl, which perhaps accounts for the fact that a nearly developed profile exists at only 2 ft from the downstream edge of the roughness in the present study compared to the 3 ft required in their experiment. Only a spectrum analysis of the turbulent fluctuations of velocity can

fully answer the first question posed above; however, comparison of the mean velocity profiles of Klebanoff and Diehl and those obtained in this study indicates that the roughness effects have been practically dissipated before reaching the first reference station. As a consequence, the parameters x_r/δ_N^* and y_r/δ_N^* in Eq 2 will not be treated further.

The plot of $\frac{U}{U_*}$ against $\log\frac{U_* y}{\nu}$ appearing in Fig. 8 which covers values of $\frac{U}{U_a}$ up to about 0.7 may be used to answer the second question listed on the previous page. Clauser (2:7) uses an equation represented by the straight line to represent the distribution of mean velocity for the "inner" region of a fully developed turbulent boundary layer. Data from this study for ambient velocities of 17 and 35 fps follow the curve in the region beyond appreciable viscous influence; however, this is not true for ambient velocities of 6 and 10 fps. Thus, it appears as though a fully developed turbulent boundary layer is not attained until $R_{\delta_N^*}$ has a value of about 2200.

Vertical Distribution of Eddy Viscosity

The primitive analysis for ϵ_N in Chapter II indicates as a result of Eq 9 that the Boussinesq number is expected to be a product of $(U_*/U_a)^2$, $R_{\delta_N^*}$ and a function of y/δ_N^*. To verify the dependence on $R_{\delta_N^*}$, values of $(\epsilon_N/\nu)(U_a/U_*)^2$ were plotted against $(R_{\delta_N^*})^{-1}$ for $y/\delta_N^* = 3$. This in effect reduces the function G to a constant. Fig. 9 shows an essentially linear variation for $R_{\delta_N^*}$ larger than about 1400 -- $(R_{\delta_N^*})^{-1}$ less than about 7×10^{-4} -- with

a slope of $-\frac{2}{3}$ rather than -1 as predicted by Eq 9. However, one notes that the data for U_a = 35 fps only may be approximately represented by a straight line having a slope of -1. Hence it appears that the turbulent shear is expressed by a universal function of y/δ^*_N only for values of $R_{\delta^*_N}$ greater than about 4000. With an exponent for $R_{\delta^*_N}$ of 3/2 determined by the slope of the solid straight line in Fig. 9, the form of G is shown in Fig. 10. Only data for $R_{\delta^*_N} > 1590$ are shown. As a result of Fig. 10, one arrives at the empirical result

$$\frac{\epsilon_N}{\nu} = 0.190\left(\frac{U_*}{U_a}\right)^2\left(R_{\delta^*_N}\right)^{3/2} \qquad 2.5 < y/\delta^*_N < 5 \ . \tag{20}$$

Thus, the Boussinesq number is nearly constant over a major portion of δ_N.

The exponent of $R_{\delta^*_N}$ in Eq 9 is unity whereas the exponent in Eq 20 is 3/2. The more rapid rate of increase in ϵ_N with $R_{\delta^*_N}$ than that predicted by Eq 9 is attributed to the changing structure of the turbulence as development nears completion.

A comparison is made in Fig. 11 of the value of $\epsilon_N/(U_a \delta_N)$ when dU/dy is calculated through the use of the logarithmic expression for the mean velocity distribution, through the use of Reichardt's modified logarithmic distribution and by graphical differentiation of the measured velocity distribution curves. In all cases $\overline{uv}$ is taken from the experimental measurements and k is taken to be 0.44. Considering the curve c as correct, the use of Eq 10 which yields curve a appears very unsatisfactory since an error at about 100 per cent results. The curve b resulting from the use of Eq 11, while giving about the

correct maximum magnitude for $\epsilon_N/(U_a \delta_N)$, yields values which are too small for y/δ_N near unity. The foregoing comparisons provide a test of the two velocity distribution equations to give correct first derivatives for use in calculating ϵ when $\overline{uv}$ is determined by measurement. One may conclude that Reichardt's representation gives an adequate method of calculating dU/dy while the standard logarithmic equation does not.

Flow Field with a Lapse

Vertical Distribution of Mean Velocity

Vertical distributions of mean velocity under lapse conditions showed only relatively minor deviations from the corresponding vertical distributions in neutral flow. Consequently, no attempt was made to determine an empirical relation for Eq 14. The deviations which appear are significant when considering similarity with flow in the atmospheric surface layer; therefore, the mean velocity data for both neutral and lapse conditions are presented in Figs. 12, 13, 14 and 15. In examining these data, one notes that without exception mean velocities for a lapse are less than or equal to those for neutral conditions at all stations except at $x = 9.30$ ft. This effect is a direct result of the increased skin friction when heat is transferred from the plate to the turbulent boundary layer. Estimated values of c_f under conditions of heating are shown in Fig. 15 of Scientific Report No. 1 (9:39).

A most significant observation from Figs. 12, 13, 14 and 15 is made when $x = 9.30$ ft for all ambient velocities except $U_a = 17$

fps. At $x = 9.30$ ft the straight line portion of the velocity profile under neutral conditions -- the portion following the logarithmic distribution -- ceases to follow the logarithmic distribution when a lapse exists and becomes concave upward in the semi-logarithmic representation. The significance of this is in the fact that similar variations occur in the atmospheric surface layer. This is illustrated by Fig. 16 which shows velocity profiles and temperature profiles measured by Halstead (3:48). The profiles representing data averaged over one hour intervals are typical of what is commonly found in the atmospheric surface layer -- Sutton (12:234). The mean velocity profiles which are concave downward accompany an inversion, the straight line distribution is characteristic of neutral conditions, and the profiles which are concave upward are typical under lapse conditions. In meteorological practice an effort is made to account for stability effects upon the mean velocity by expressing U as a power function of the height while relating the exponent to a stability parameter such as the Richardson number. Before this can be done for wind tunnel velocity profiles, a greater range of the stability parameters must be attained. Such a program has been initiated at Colorado A and M College with the construction of a wind tunnel having an 80-ft long test section to permit formation of very thick turbulent boundary layers.

One consistent characteristic of the profiles at $x = 9.30$ ft is a crossing of the neutral and lapse profiles below $y = 0.2$ in . This is a result of the large viscous forces near the surface of the smooth plate and is rarely, if ever, observed in micrometeorological

data. With few exceptions, the natural surfaces encountered in the field are aerodynamically rough; therefore, wind tunnel studies of lapse effects in which the viscous forces are minimized by roughening the surface are needed.

Vertical Distribution of Mean Temperature

Mean temperature profiles are shown in Figs. 17, 18, 19, 20 and 21. The object of these representations is to determine what degree of similarity exists for Θ as a function of the variable y/δ_t^*. Here the temperature displacement thickness δ_t^* is a variable analogous to the velocity displacement thickness δ_N^*. Similarity does not exist in terms of the simple similarity parameter y/δ_t^* for the temperature distributions at different values of R_x keeping U_a constant. Apparently complete similarity exists only in terms of a complex similarity parameter involving R_x and $F_{\delta_N^*}$ as well as y/δ_t^*. The results shown in Fig. 21 are significant in that a good degree of similarity is achieved for Θ in terms of the parameter y/δ_t^* at $x = 9.30$ ft for all U_a. The condition which is met in all these separate situations except for $U_a = 6$ fps is that $\delta_L \leq \delta_t$.

Comparing mean velocity distributions in Fig. 8 with the temperature distributions of Fig. 21 excellent similarity is observed except in the region where viscous forces and molecular heat transfer are relatively large.

Vertical Distribution of Eddy Viscosity

The effects of stability upon the eddy viscosity and the closely related eddy conductivity and diffusivity are of considerable practical importance; therefore, an effort is made to determine the proper exponents appearing in Eq 18.

Figs. 22, 23, 24 and 25 were prepared to allow comparisons to be made of the absolute values of ϵ_N and ϵ_L as the thermal boundary layer develops for different ambient velocities and temperature differences. In all cases, the maximum value of ϵ_L increases with R_x . This observation is, of course, confined to the range of R_x in the tests which cover the growth of δ_t from zero to δ_L . Another consistent variation is an increase in ϵ_L with R_{δ_N} with the exception of data for $x = 0.29$ ft , 0.96 ft and 3.29 ft at an ambient velocity of 10 fps. Values of ϵ_L being larger for $U_a = 10$ fps at $x = 0.29$ ft , 0.96 ft and 3.29 ft than for $U_a = 17$ fps at corresponding values of x is attributed to the larger $\Delta T/T_o$ values for $U_a = 10$ fps -- see Table II. Values of ϵ_L for $x = 0.29$ ft and 0.96 ft should not be given the same confidence as for $x = 3.29$ ft and 9.30 ft since large variations of the quantities being measured occur across the hot-wire probe because of the large gradients and the large hot-wire probe dimensions.

In order to determine proper exponents n_1 , n_2 , and n_3 for Eq 18, n_2 was set equal to zero on the grounds that the ambient velocities studied were of such a magnitude that the ratio of inertia forces to buoyancy forces as characterized by the Froude number is more

significant than the ratio of buoyancy forces to viscous forces as measured by the Grashof number. Fig. 26 represents the values of $(\epsilon_L - \epsilon_N)/\nu_0$ taken from the curves of Figs. 22, 23, 24 and 25 for $y/\delta_N^* = 3$. This procedure reduces ϕ to a constant value for all points shown. The value of 1/4 for n_3 was obtained by trial and error in an attempt to reduce the scatter of values of $\frac{\epsilon_L - \epsilon_N}{\nu_0} (F_{\delta_N^*})^{n_3}$ plotted against R_x. With the exception of points for $U_a = 10$ fps, and the uncertain points for $x = 0.29$ ft and 0.96 ft, the deviation from the straight line selected to represent the data is within the estimated error of measurement. Having determined the exponent n_1 to be unity from Fig. 26, entire vertical distributions of $\frac{\epsilon_L - \epsilon_N}{\nu_0}$ are shown in Fig. 27. The function $\phi(y/\delta_N^*)$ cannot be determined from Fig. 27; therefore, one can only write

$$\frac{\epsilon_L - \epsilon_N}{\nu_0} = \left(F_{\delta_N^*}\right)^{-1/4} R_x \phi\left(\frac{y}{\delta_N^*}\right) = \left|Ri_{\delta_N^*}\right|^{1/8} R_x \phi\left(\frac{y}{\delta_N^*}\right) \quad . \qquad (21)$$

This means that the difference in the Boussinesq number for vertical and lapse conditions increases as the ratio of buoyancy forces to inertia forces taken to the 1/8 power and directly with the heating length Reynolds number for the particular conditions of these studies. One should note that the dependence upon R_x is essentially for the condition $\delta_t \leq \delta_L$ and should not be used for cases in which $\delta_t > \delta_L$ until further measurements for these extended conditions can be made.

Effect of Lapse upon the Correlation Coefficient

The correlation coefficient $\overline{uv}/u'v' = r$ for both the neutral and lapse conditions is shown as a function of y in Figs. 28, 29, 30 and 31. These data represent direct hot-wire measurements of velocity fluctuations and show the usual large amount of scatter. Because of the scatter, definite conclusions regarding the effect of lapse on the data are difficult to make. One consistent result is an increase in r_L compared to r_N for sufficiently large y/δ^*_L. Such a result appears reasonable as an effect of heated parcels of air rising through the boundary layer. It is worthy to note also that the maximum value of r_N for all but the 10 fps data is near -0.53 which is in good agreement with the values found in the atmospheric surface layer by Scrase as given by Sutton (12:262).

Effect of Lapse upon the Isotropy Ratio

The ratio u'/v' is a measure of how nearly isotropic the turbulence field is. Figs. 32, 33, 34 and 35 show $(u'/v')_N$ and $(u'/v')_L$ as functions of y. With the exception of data at $x = 0.29$, the flow becomes less isotropic for lapse conditions. A value of $(u'/v')_N \sim 2$ over the central portion of the boundary layer agrees well with values obtained by Best over grassland -- Sutton (12:254).

Effect of Lapse upon the Mixing Length and Mixing Velocity-Mixing Length Ratio

The mixing length is increased from 100 to 400 per cent as a result of the lapse conditions encountered in these tests. Fig. 36

shows the increase in ℓ/δ^*_N due to heating. If one considers turbulence to be a system of vortices being generated near the surface and then moving upward through the fluid, the increase in mixing length with heating may be attributed to the greater vertical acceleration resulting from the buoyancy forces and hence the greater distance most vortices travel before dissipation.

The ratio v'/ℓ appears in Lettau's approach for expressing ϵ_L in terms of ϵ_N -- Hewson (4:68). The assumption used is that $(v'/\ell)_N = (v'/\ell)_L$. Fig. 37 shows values of both ratios as a function of y/δ^*_N . For each ambient velocity except 10 fps, $(v'/\ell)_L < (v'/\ell)_N$ above the region of large viscous forces. Atmospheric surface layer data adequate to determine whether the same effect occurs there is not known to exist.

Intensity of Temperature Fluctuations

Because of the essentially one dimensional nature of the temperature fluctuation probe, the gradients of fluctuation as given by Figs. 38, 39, 40 and 41 are realistic. Especially near the boundary, except when $U_a = 35$ fps , the rapidly changing nature of the flow becomes apparent. The maximum temperature fluctuation intensity in most cases decreases with x . This apparently is a result of decreasing vertical temperature gradients as the thermal boundary layer penetrates more deeply into the momentum boundary layer. In the case of the maximum value of $T'/\Delta T$ in going from $x = 0.29$ to 3.29 for $U_a = 6$ fps and $x = 0.29$ to 0.96 for $U_a = 10$ fps there is an increase. In

checking the value of y at which the maximum of $T'/\Delta T$ occurs in these cases it becomes apparent that for $x < 0$ there is a thick laminar sub-layer which becomes unstable and decomposes into a relatively thin layer at some value of $x > 0$. This mechanism accounts for the anomalous variation in the maximum value of $T'/\Delta T$ for small values of x at these low ambient velocities.

In comparing the distributions of v'/U_o and $T'/\Delta T$ one notes the general similarity of a continuous decrease in magnitude after passing through a maximum near the boundary; however, the values of v'/U_o are consistently about twice the value of $T'/\Delta T$ at corresponding locations and similar flow and thermal characteristics.

IV. CONCLUSIONS

As a result of this study of turbulent flow over smooth, plane, horizontal, heated and unheated boundaries, several significant conclusions may be reached. These conclusions which are valid for a range of ambient velocity of 6 to 35 fps, moderate temperature differences of 60 to 120°F and a heated plate length of 10 ft are as follows:

1. For neutral flow, the distribution of eddy viscosity ϵ_N is approximated by

$$\frac{\epsilon_N}{\nu} = 0.190 \left(\frac{U_*}{U_a} \right)^2 \left(R \delta_N^* \right)^{3/2}$$

for $2.5 < y/\delta_N^* < 5$. This result should be considered as applicable only when $1600 < R \delta_N^* < 6400$.

2. Mean velocity profiles under lapse conditions in the wind tunnel show the same typical change of curvature as do mean velocity profiles for the atmospheric surface layer with a lapse. Only above a height over the smooth boundary at which the viscous forces become negligible does this similarity hold; therefore, if atmospheric surface layer similarity is to be improved, wind tunnel boundaries should be roughened.

3. Eddy viscosity under lapse conditions ϵ_L can be correlated with ϵ_N within the range of these studies through the expression

$$\frac{\epsilon_L - \epsilon_N}{\nu_o} = \left(\mathrm{F}\,\delta_N^*\right)^{-1/4} R_x \emptyset\left(\frac{y}{\delta_N^*}\right) = \left|\mathrm{Ri}\,\delta_N^*\right|^{1/8} R_x \emptyset\left(\frac{y}{\delta_N^*}\right)$$

4. The mean temperature distributions are similar when (y/δ_t^*) is used as a similarity parameter, provided $\delta_t \doteq \delta_L$.

In order to relate adequately a stability factor such as $\mathrm{Ri}\,\delta_N^*$ to the exponent in a velocity distribution representation which is a power function of the height y, measurements must be made over a much greater range of $\mathrm{Ri}\,\delta_N^*$ than has been possible with the equipment available for these studies. Such extended measurements in which x is increased by a factor of about 10 should permit the function $\emptyset$ relating ϵ_L and y/δ_N^* in Conclusion 3 to be determined and the exponent of R_x in the expression for $\frac{\epsilon_L - \epsilon_N}{\nu_o}$ to be evaluated for fully developed turbulent flow.

REFERENCES

1. Batchelor, G. K. Heat convection and buoyancy effects in fluids. Quarterly Journal, Royal Meteorological Society, 80:339-58, July 1954.

2. Dryden, H. L. and von Karman, Th. (Editors). Advance in applied mechanics, Vol 4. New York, N. Y., Academic Press, 1956.

3. Halstead, M. H. Experimental verification of the equations for turbulent transfer. Seabrook, N. J., The Johns Hopkins Univ., Laboratory of Climatology, Sept. 1951.
(Contract No. W28-099-ac-378, Interim Report No. 15.)

4. Hewson, E. W. (Editor). International symposium on atmospheric turbulence in the boundary layer. Cambridge, Mass., Geo. Res. Directorate, Air Force Cambridge Research Center, Air Research and Development Command, Dec 1952.
(Geo. Res. Paper No. 19)

5. Johnson, D. S. Turbulent heat transfer in a boundary layer with discontinuous wall temperature. Baltimore, Md., Office of Scientific Research, Air Research and Development Command, Aug 1955.
(Contract AF 18(600)671.)

6. Klebanoff, P. S. and Diehl, Z. W. Some features of artificially thickened fully developed turbulent boundary layers with zero pressure gradient. Washington, National Advisory Committee for Aeronautics, 1952.
(NACA Report 1110)

7. Liepmann, H. W. and Fila, G. H. Investigations of effects of surface temperature and single roughness elements on boundary layer transition. Washington, National Advisory Committee for Aeronautics, 1947.
(NACA Report 890)

8. Schlichting, H. Boundary layer theory. New York, McGraw-Hill, 1955.

9. Spengos, A. C. Turbulent diffusion of momentum and heat from a smooth, plane boundary with zero pressure gradient. Cambridge, Mass., Air Force Cambridge Research Center, Feb 1956.
(Contract No. AF 19(604)-421, TN-56-259)

10. Spengos, A. C. and Cermak, J. E. Heat transfer by forced convection from a horizontal flat plate into a turbulent boundary layer. Palo Alto, Calif., Heat Transfer and Fluid Mechanics Institute, Stanford Univ., June 1956. (Reprints 1956)

11. Spengos, A. C. and Cermak, J. E. Turbulent diffusion of momentum and heat from a smooth, plane boundary with zero pressure gradient. Final Report - Part I. Experimental Equipment. Cambridge, Mass., Air Force Cambridge Research Center, Aug 1956. (Contract AF 19(604)-421, TN-56-273)

12. Sutton, O. G. Micrometeorology. New York, McGraw-Hill, 1953.

13. Townsend, A. A. The structure of turbulent shear flow. Cambridge, Mass., Cambridge University Press, 1956.

TABLES

TABLE I

Symbol	U_a	x	T_a	δ_N	δ_N^*	U_*	$R_{\delta_N^*}$
	fps	ft	°F	in.	in.	fps	10^3
○	6.0	0.29	50.0	1.20	0.200	0.349	0.553
⊖	6.0	0.96	50.0	1.50	0.225	0.338	0.622
⊕	6.1	3.29	50.0	2.00	0.332	0.333	0.919
●	6.1	9.30	53.0	3.30	0.540	0.327	1.492
○	10.0	0.29	59.0	1.70	0.298	0.662	1.370
⊖	9.9	0.96	59.0	1.90	0.312	0.641	1.437
⊕	9.9	3.29	59.0	2.30	0.345	0.549	1.590
●	9.9	9.30	59.0	3.00	0.463	0.540	2.130
○	17.1	0.29	55.0	1.60	0.282	0.735	2.260
⊖	17.1	0.96	54.0	1.80	0.292	0.736	2.145
⊕	17.0	3.29	52.0	2.50	0.366	0.732	2.860
●	17.1	9.30	48.0	2.80	0.417	0.726	3.185
○	35.0	0.29	44.0	1.60	0.243	1.528	3.915
⊖	34.0	0.96	49.0	1.90	0.247	1.485	3.980
⊕	35.5	3.29	52.0	2.40	0.307	1.525	4.950
●	35.0	9.30	54.0	3.00	0.396	1.474	6.380

TABLE II

Symbol	U_a	x	T_a	ΔT	$\frac{\Delta T}{T_o}$	δ_L	δ_t	δ_L^*	δ_t^*	R_x	$F_{\delta_N^*}$
	fps	ft	°F	°F		in.	in.	in.	in.	10^4	
●	6.0	0.29	65.0	110.0	0.173	2.00	0.45	0.445	0.077	0.66	19.7
●	6.0	0.96	68.0	107.5	0.169	2.40	0.70	0.479	0.125	2.18	18.0
●	6.0	3.29	69.0	100.0	0.159	3.60	2.00	0.589	0.294	7.38	14.2
●	6.0	9.30	72.0	93.5	0.150	7.30	5.90	0.972	0.886	21.80	12.9
●	10.0	0.29	70.0	118.0	0.182	1.80	0.60	0.319	0.074	1.06	26.2
●	9.8	0.96	74.0	112.0	0.174	2.00	1.30	0.353	0.147	3.45	25.7
●	9.8	3.29	75.0	111.3	0.172	2.20	2.30	0.399	0.259	11.80	24.5
●	9.2	9.30	72.0	106.7	0.167	2.80	4.00	0.501	0.600	31.30	19.6
●	16.1	0.29	50.0	93.0	0.154	1.80	0.45	0.292	0.085	1.96	47.8
●	17.0	0.96	51.0	90.3	0.150	2.20	0.95	0.381	0.136	6.87	47.8
●	16.7	3.29	52.0	85.0	0.142	2.50	2.00	0.428	0.254	23.10	44.5
●	17.0	9.30	50.0	82.0	0.139	3.80	4.00	0.634	0.634	66.50	43.1
●	35.7	0.29	64.0	62.0	0.106	1.60	0.30	0.260	0.048	4.48	135.6
●	34.8	0.96	67.0	61.3	0.104	1.80	0.70	0.286	0.090	14.48	132.5
●	34.0	3.29	63.0	60.0	0.103	2.50	1.70	0.362	0.322	48.30	116.5
●	34.0	9.30	60.0	58.3	0.101	4.00	4.00	0.516	0.662	137.00	104.0

FIGURES

Fig.

1 Plan of wind tunnel

2 Definition sketch for momentum and thermal boundary layers

3 Verticial profiles of shear stress, vertical and longitudinal intensities of turbulence for U_a = 6 fps

4 Mean velocity distributions for U_a = 35 fps with $\Delta T = 0$

5 Mean velocity distributions for U_a = 17 fps with $\Delta T = 0$

6 Mean velocity distributions for U_a = 10 fps with $\Delta T = 0$

7 Mean velocity distributions for U_a = 6 fps with $\Delta T = 0$

8 Composite of mean velocity distributions for U_a = 6, 10, 17, 35 fps with $\Delta T = 0$

9 Variation of $\frac{\epsilon_N}{\nu}(U_a/U_*)^2$ with $\left(R\,\delta_N^*\right)^{-1}$ for $y/\delta_N^* = 3$

10 Variation of $\frac{\epsilon_N}{\nu}(U_a/U_*)^2 \left(R\,\delta_N^*\right)^{-3/2}$ with y/δ_N^*

11 Comparison of eddy viscosity distributions for $\Delta T = 0$
   a) dU/dy from logarithmic velocity distribution
   b) dU/dy from modified logarithmic velocity distribution
   c) dU/dy from graphical differentiation of measured velocity distribution

12 Variation of U_N and U_L for U_a = 35 fps

13 Variation of U_N and U_L for U_a = 17 fps

14 Variation of U_N and U_L for U_a = 10 fps

15 Variation of U_N and U_L for U_a = 6 fps

16 Variation of mean velocity distribution in the atmospheric surface layer with stability -- Halstead (3:48)

Fig.

17 Mean temperature distributions for U_a = 35 fps

18 Mean temperature distributions for U_a = 17 fps

19 Mean temperature distributions for U_a = 10 fps

20 Mean temperature distributions for U_a = 6 fps

21 Comparison of mean temperature distributions for x = 9.30 ft

22 Variation of ϵ_N and ϵ_L for U_a = 35 fps

23 Variation of ϵ_N and ϵ_L for U_a = 17 fps

24 Variation of ϵ_N and ϵ_L for U_a = 10 fps

25 Variation of ϵ_N and ϵ_L for U_a = 6 fps

26 Variation of $(\epsilon_L - \epsilon_N)/\nu_o \quad F\,\delta_N^{*1/4}$ with R_x for $y/\delta_N^* = 3$

27 Variation of $(\epsilon_L - \epsilon_N)/\nu_o \quad F\,\delta_N^{*1/4}\,R_x^{-1}$ with y/δ_N^*

28 Variation of r_N and r_L for U_a = 35 fps

29 Variation of r_N and r_L for U_a = 17 fps

30 Variation of r_N and r_L for U_a = 10 fps

31 Variation of r_N and r_L for U_a = 6 fps

32 Variation of $(u'/v')_N$ and $(u'/v')_L$ for U_a = 35 fps

33 Variation of $(u'/v')_N$ and $(u'/v')_L$ for U_a = 17 fps

34 Variation of $(u'/v')_N$ and $(u'/v')_L$ for U_a = 10 fps

35 Variation of $(u'/v')_N$ and $(u'/v')_L$ for U_a = 6 fps

36 Variation of $(\ell/\delta_N^*)_N$ and $(\ell/\delta_N^*)_L$ for x = 9.30 ft

37 Variation of $(v'/\ell)_N$ and $(v'/\ell)_L$ for x = 9.30 ft

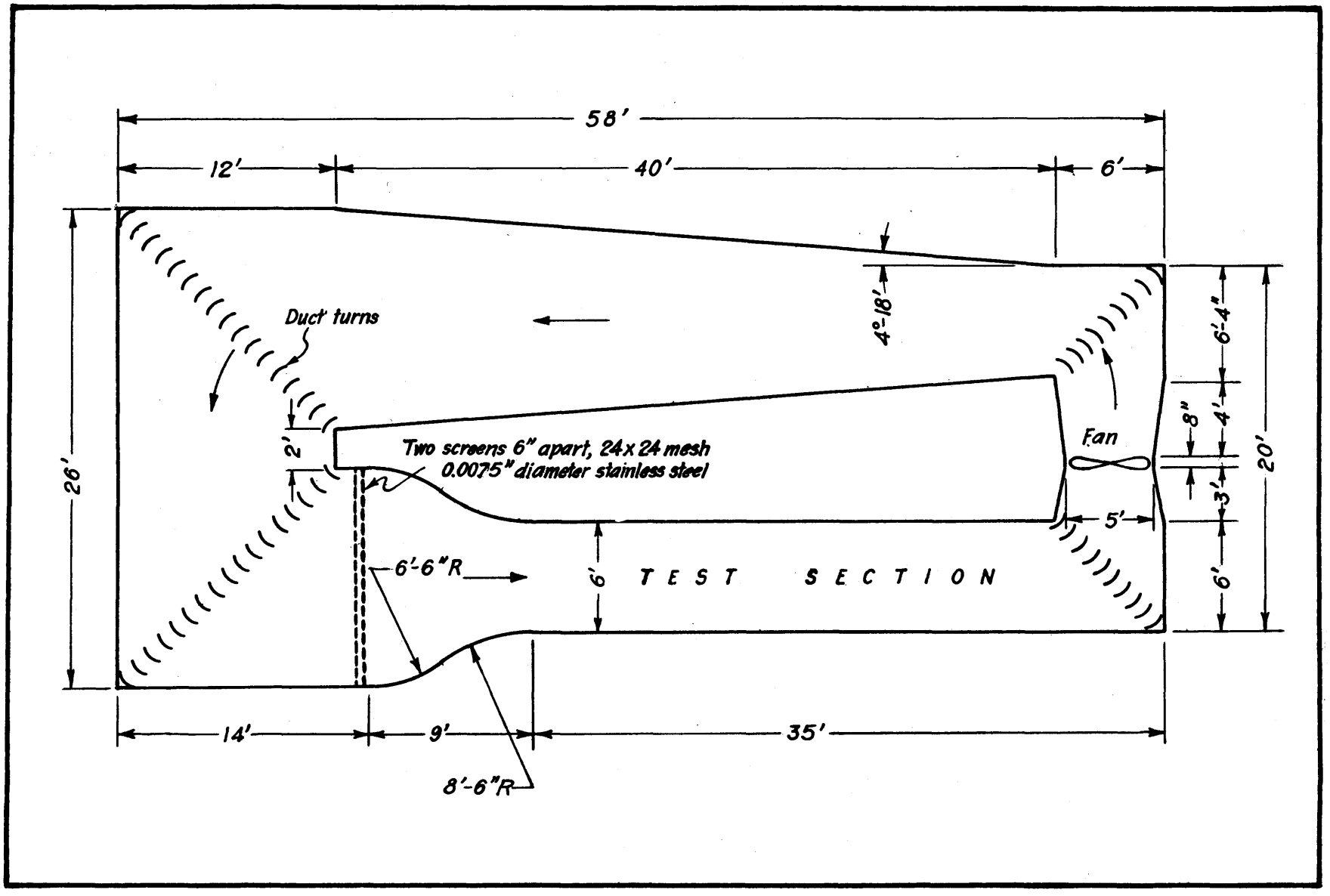

Fig. 1 Plan of wind tunnel

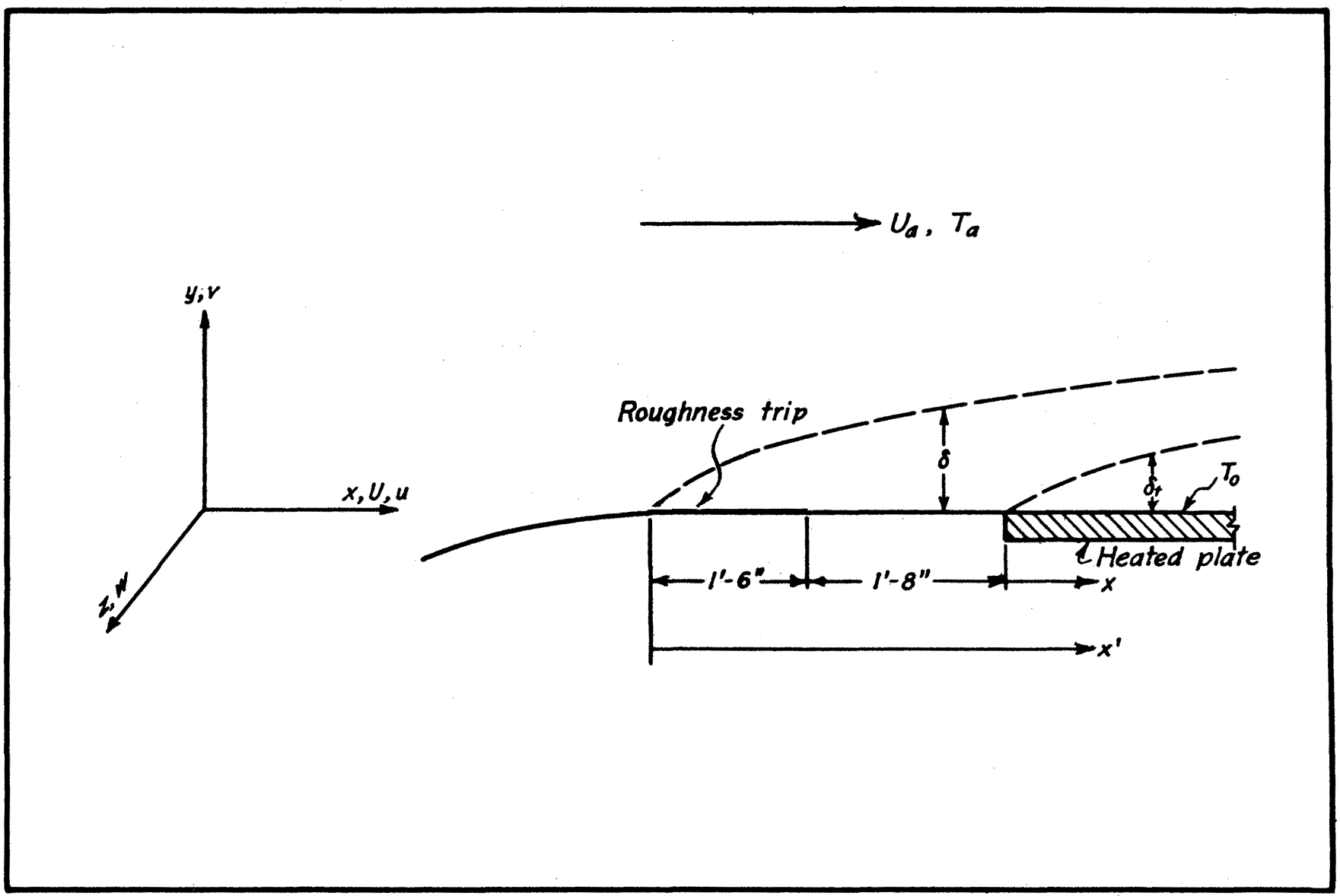

Fig. 2 Definition sketch for momentum and thermal boundary layers

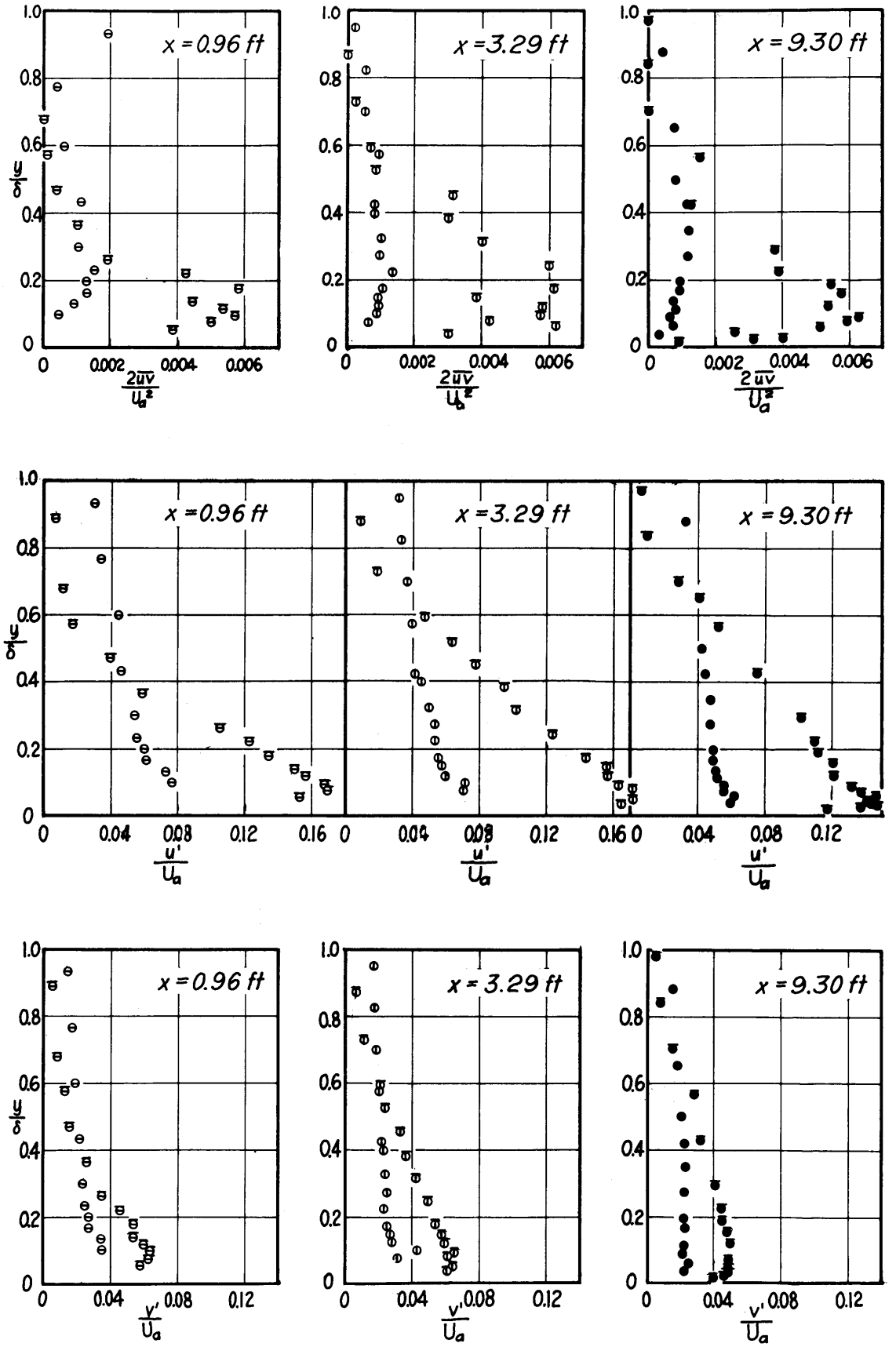

Fig. 3 Vertical profiles of shear stress, vertical and longitudinal intensities of turbulence for U_a=6 fps

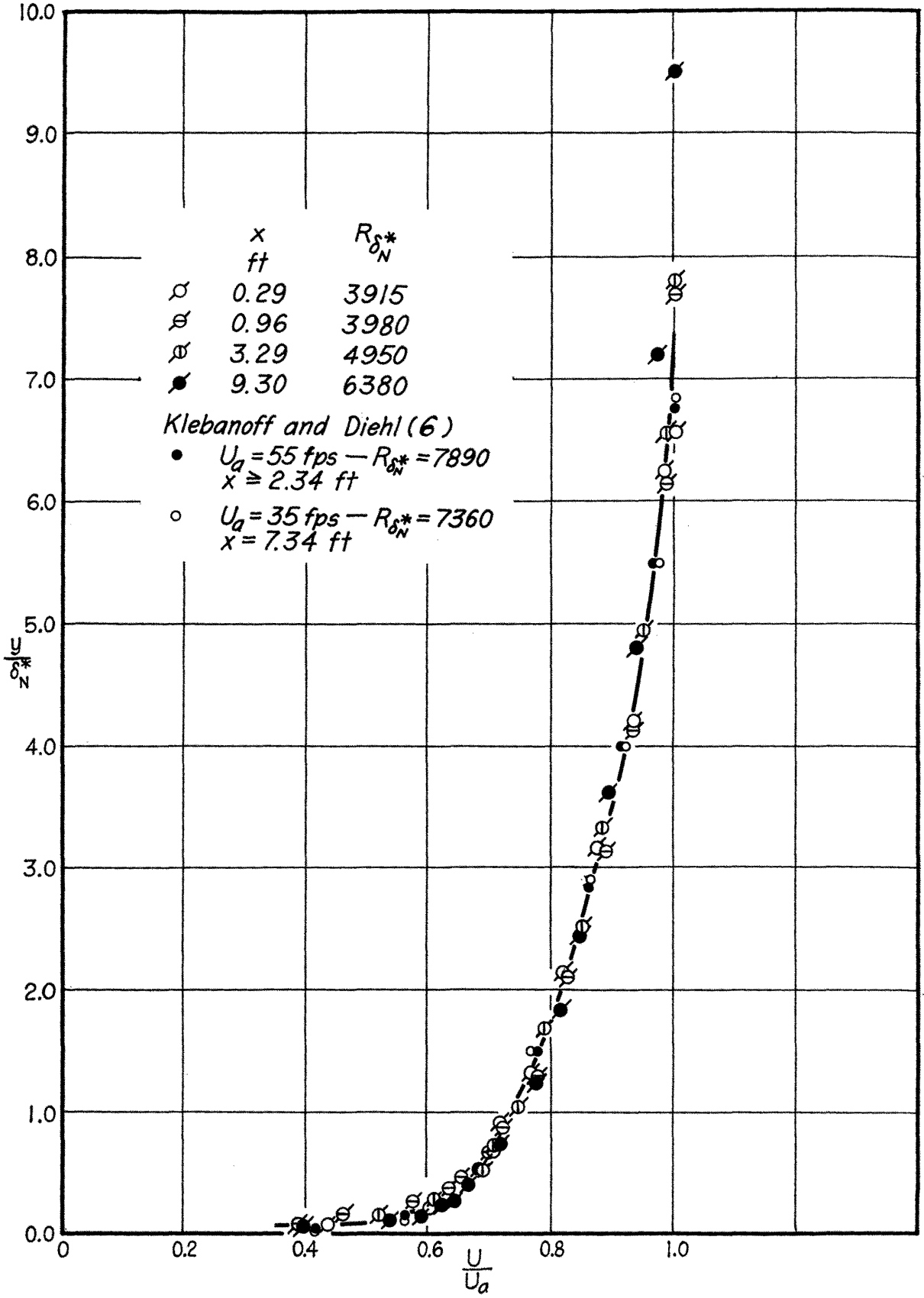

Fig. 4 Mean velocity distribution for $U_a = 35$ fps with $\Delta T = 0$

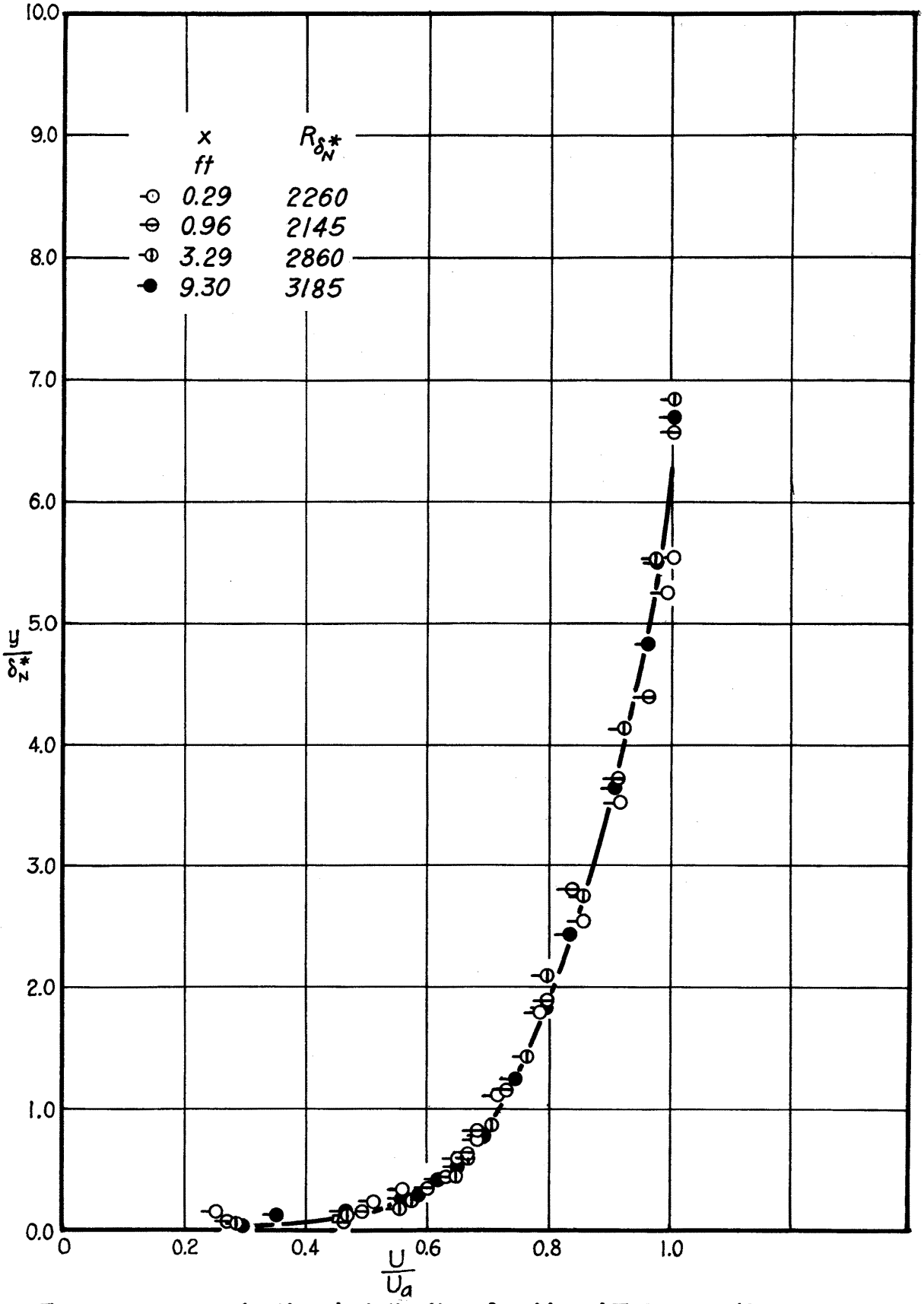

Fig. 5 Mean velocity distribution for $U_a = 17$ fps with $\Delta T = 0$

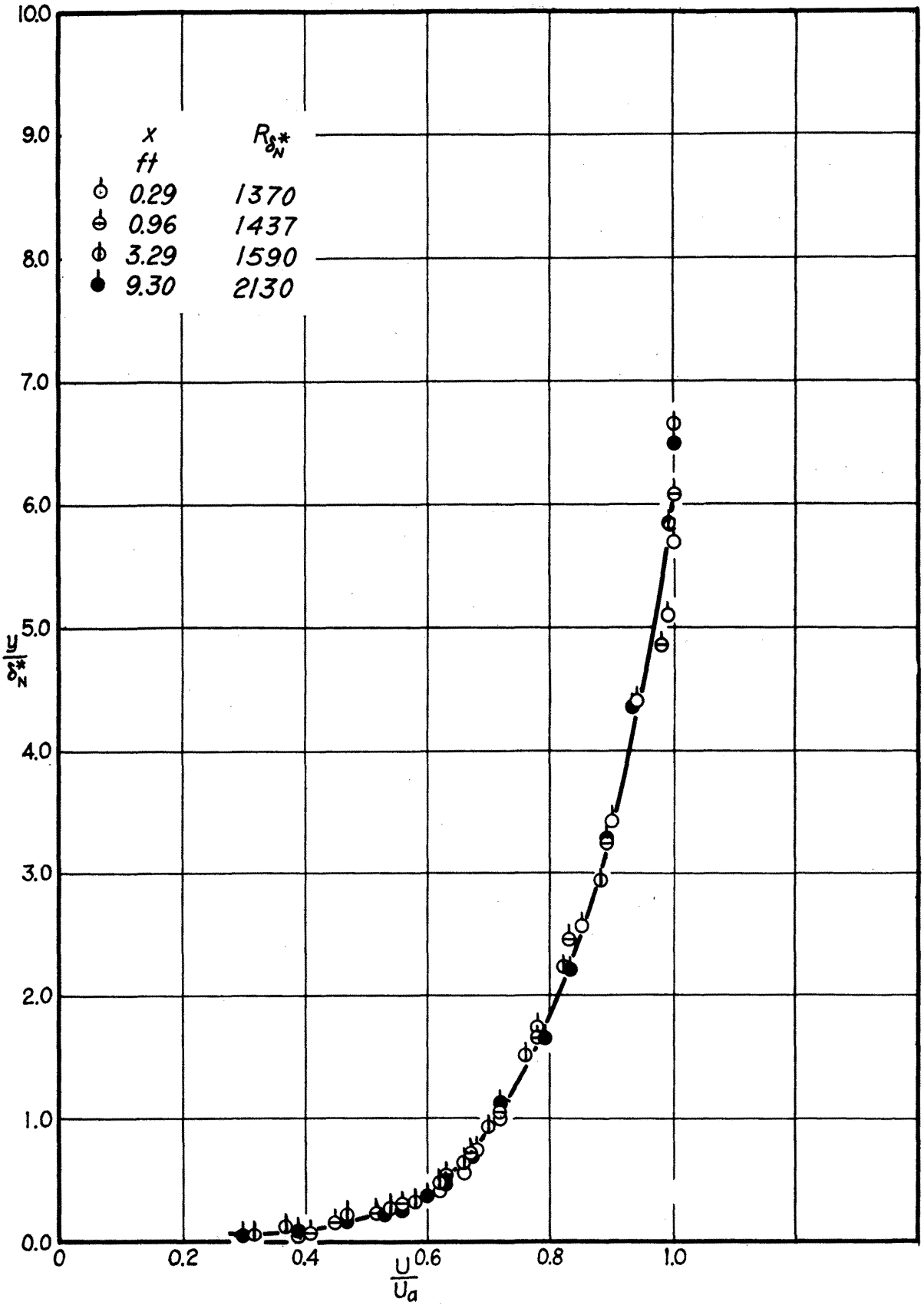

Fig. 6 Mean velocity distribution for U_a=10 fps with ΔT=0

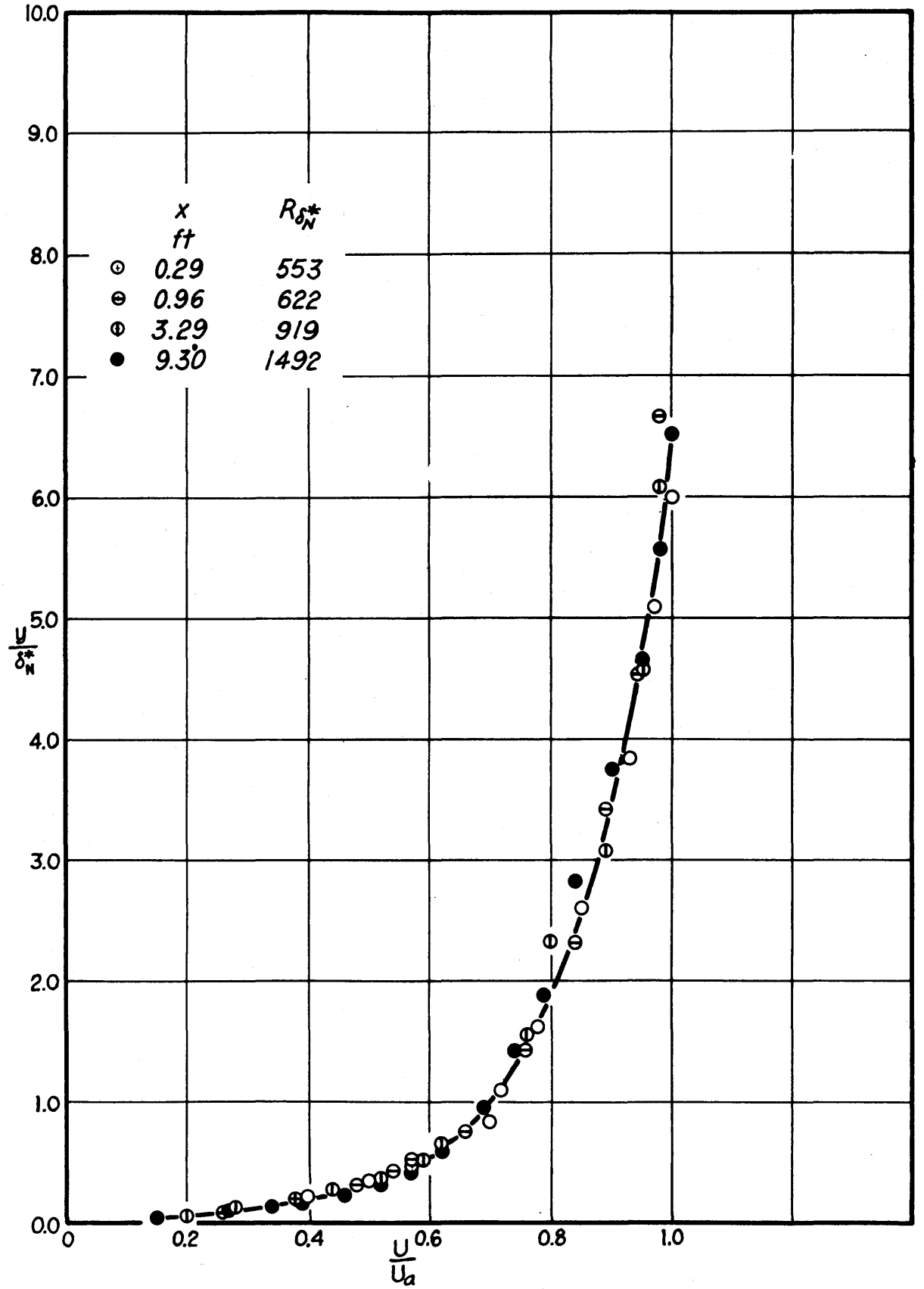

Fig. 7 Mean velocity distribution for $U_a = 6$ fps with $\Delta T = 0$

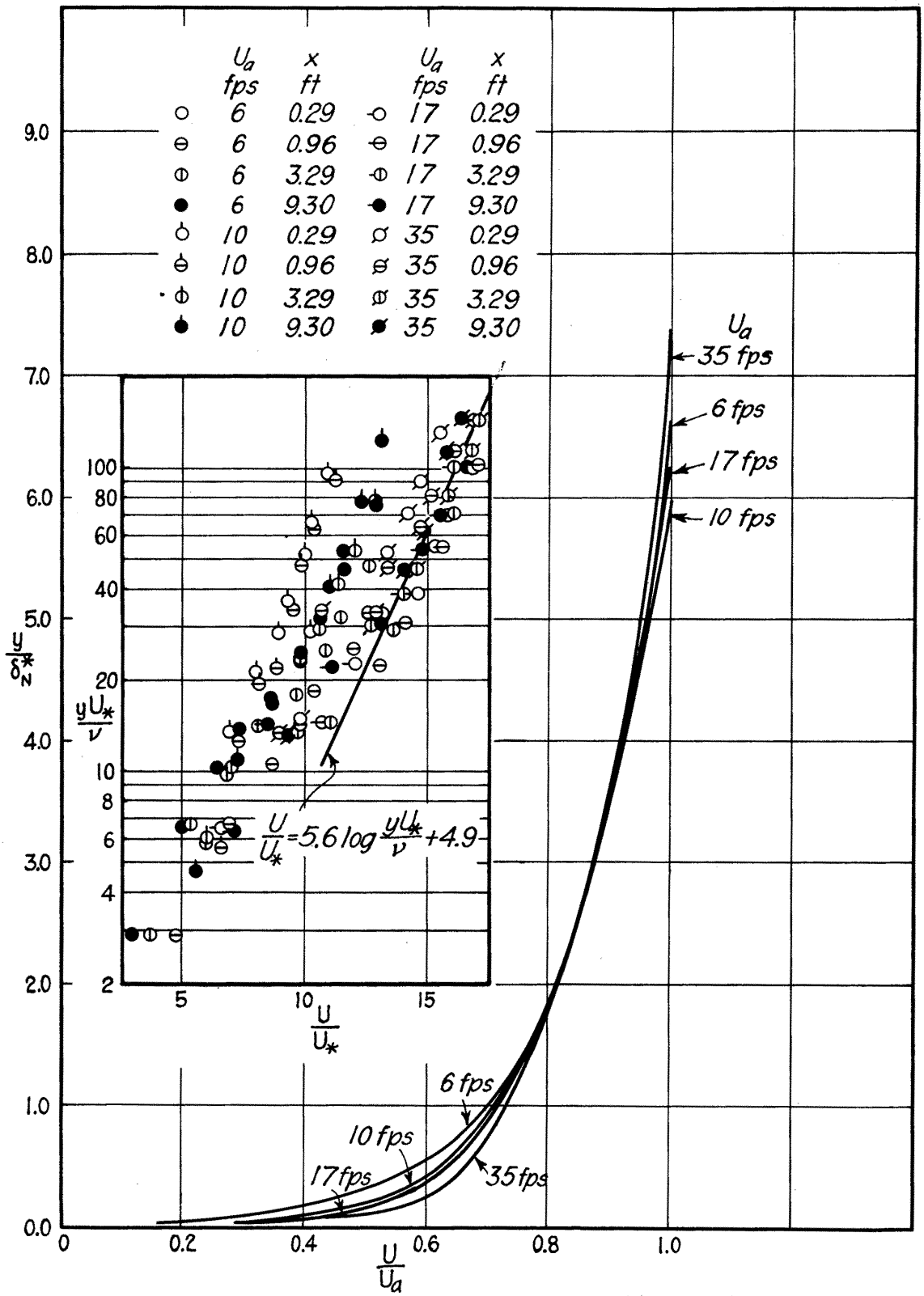

Fig. 8 Composite of mean velocity distributions for $U_a = 6, 10, 17, 35$ fps with $\Delta T = 0$.

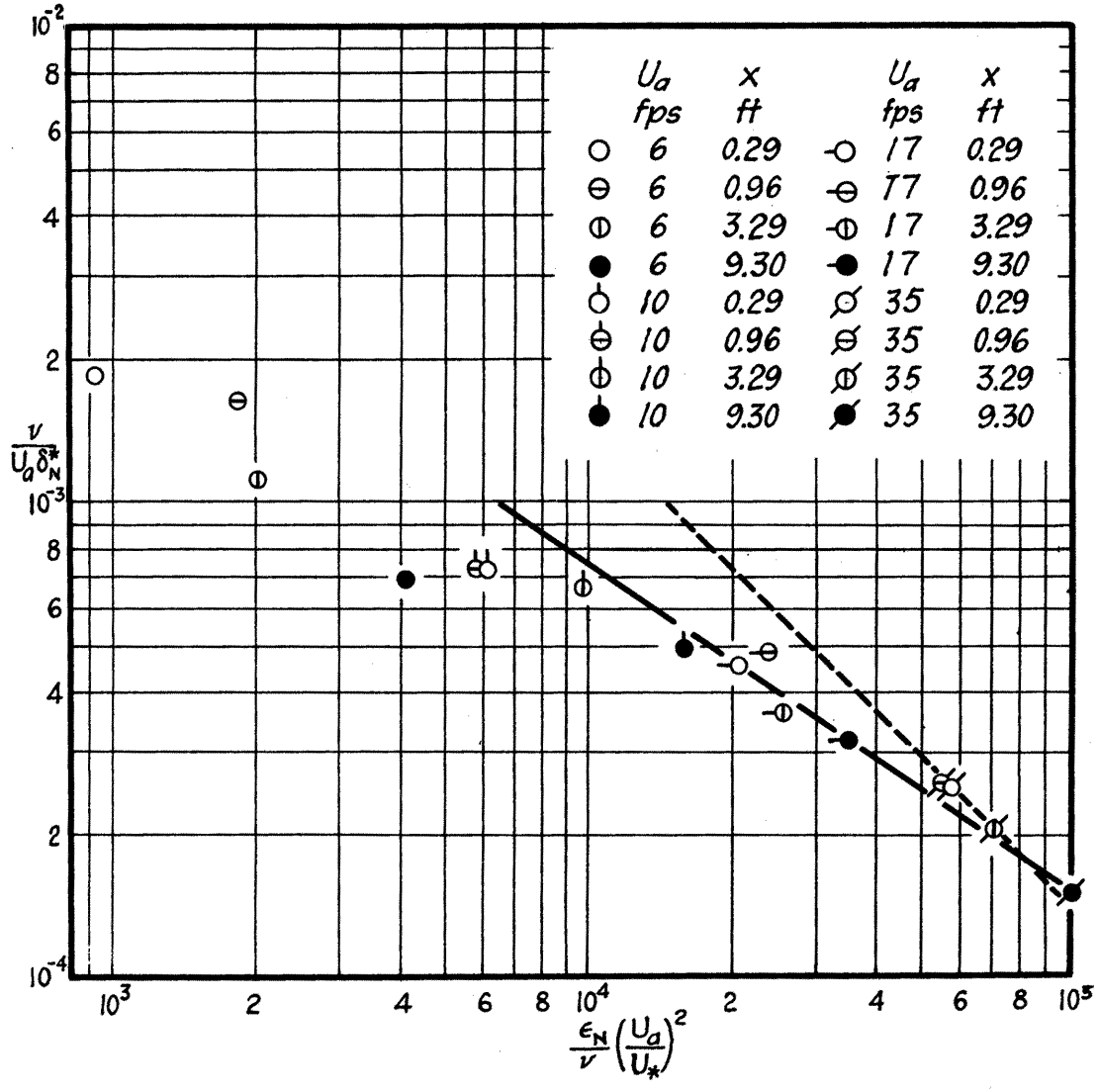

Fig. 9 Variation of $\frac{\epsilon_N}{\nu}\left(\frac{U_a}{U_*}\right)^2$ with $R_{\delta_N^*}^{-1}$ for $\frac{y}{\delta_N^*}=3$

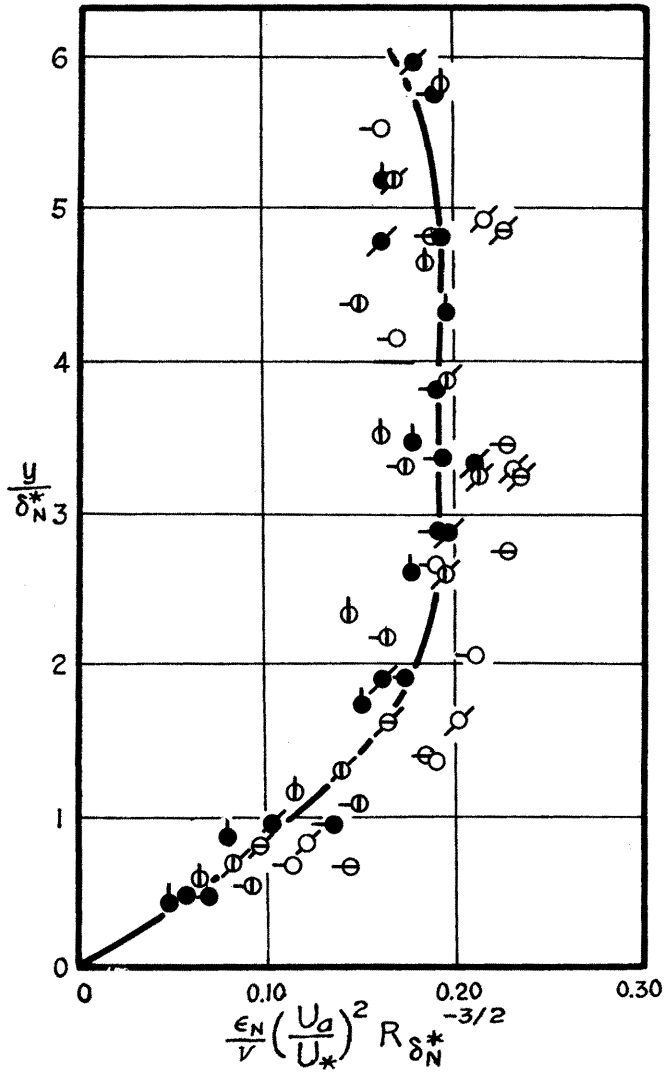

Fig. 10 Variation of $\frac{\epsilon_N}{\nu}\left(\frac{U_a}{U_*}\right)^2 R_{\delta_N^*}^{-3/2}$ with $\frac{y}{\delta_N^*}$

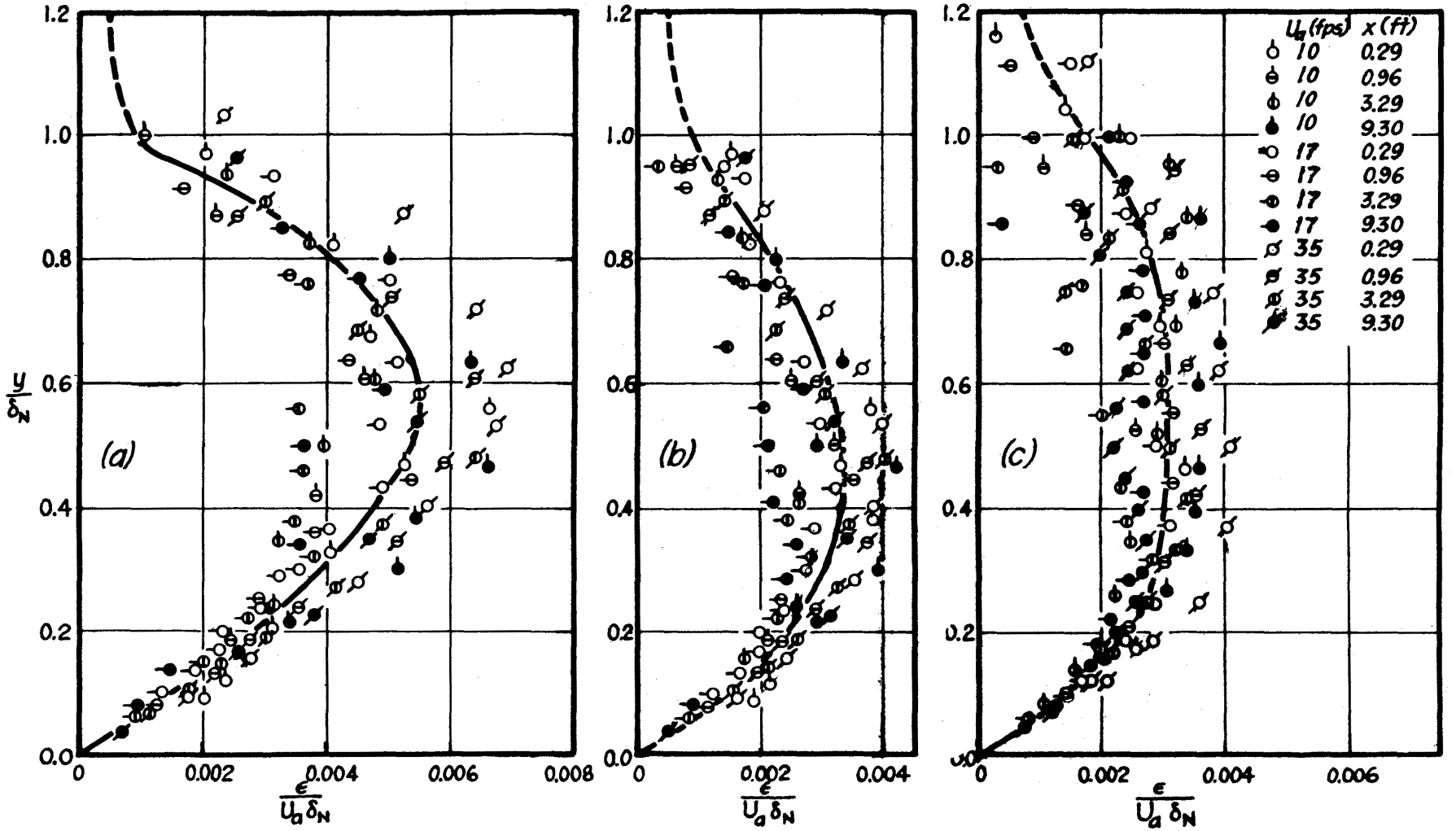

Fig. 11 Comparison of eddy viscosity distributions for $\Delta T = 0$
(a) dU/dy from logarithmic velocity distribution
(b) dU/dy from modified logarithmic velocity distribution
(c) dU/dy from graphical differentiation of measured velocity distribution

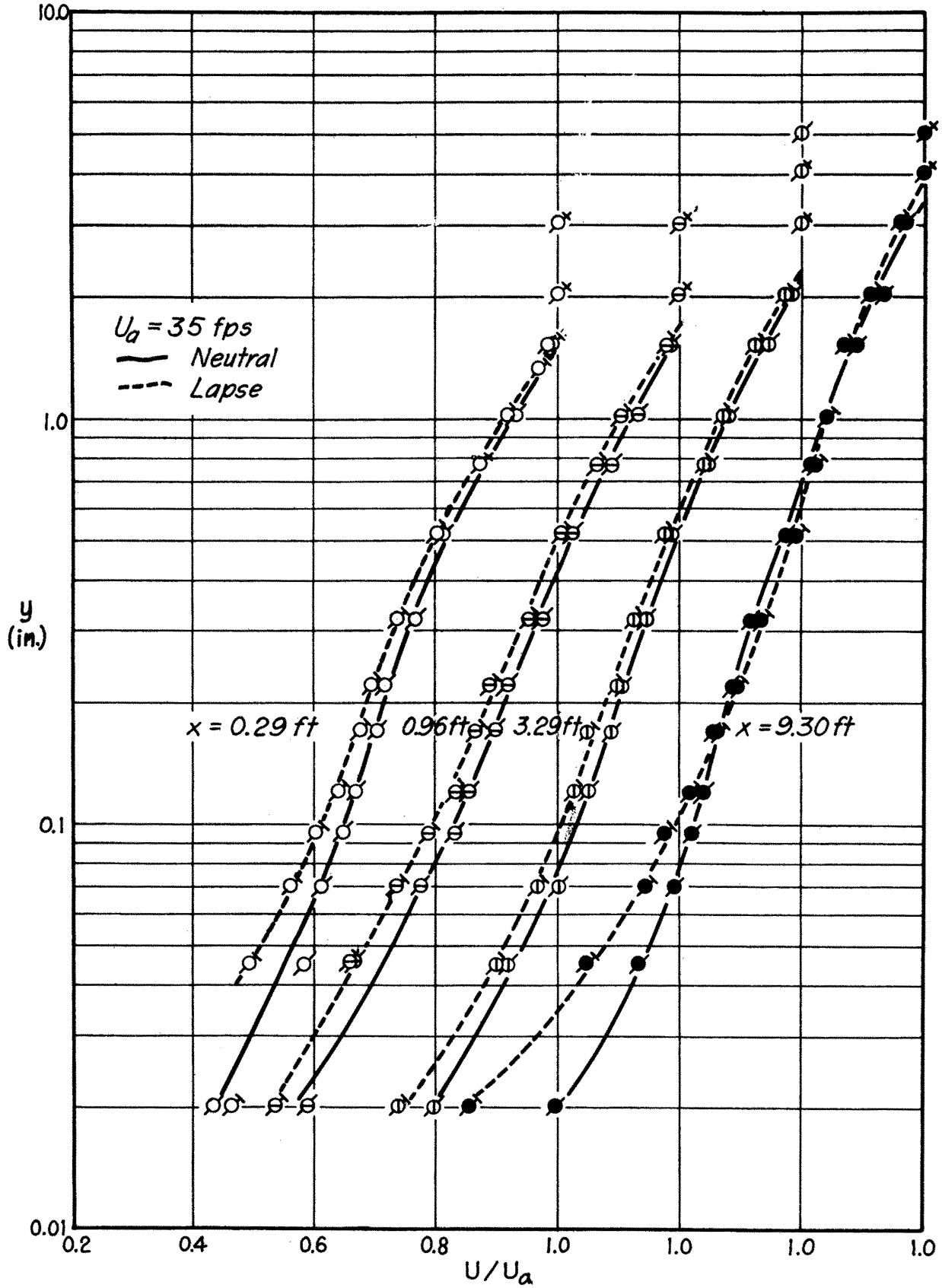

Fig. 12 Variation of U_N and U_L for U_a = 35 fps

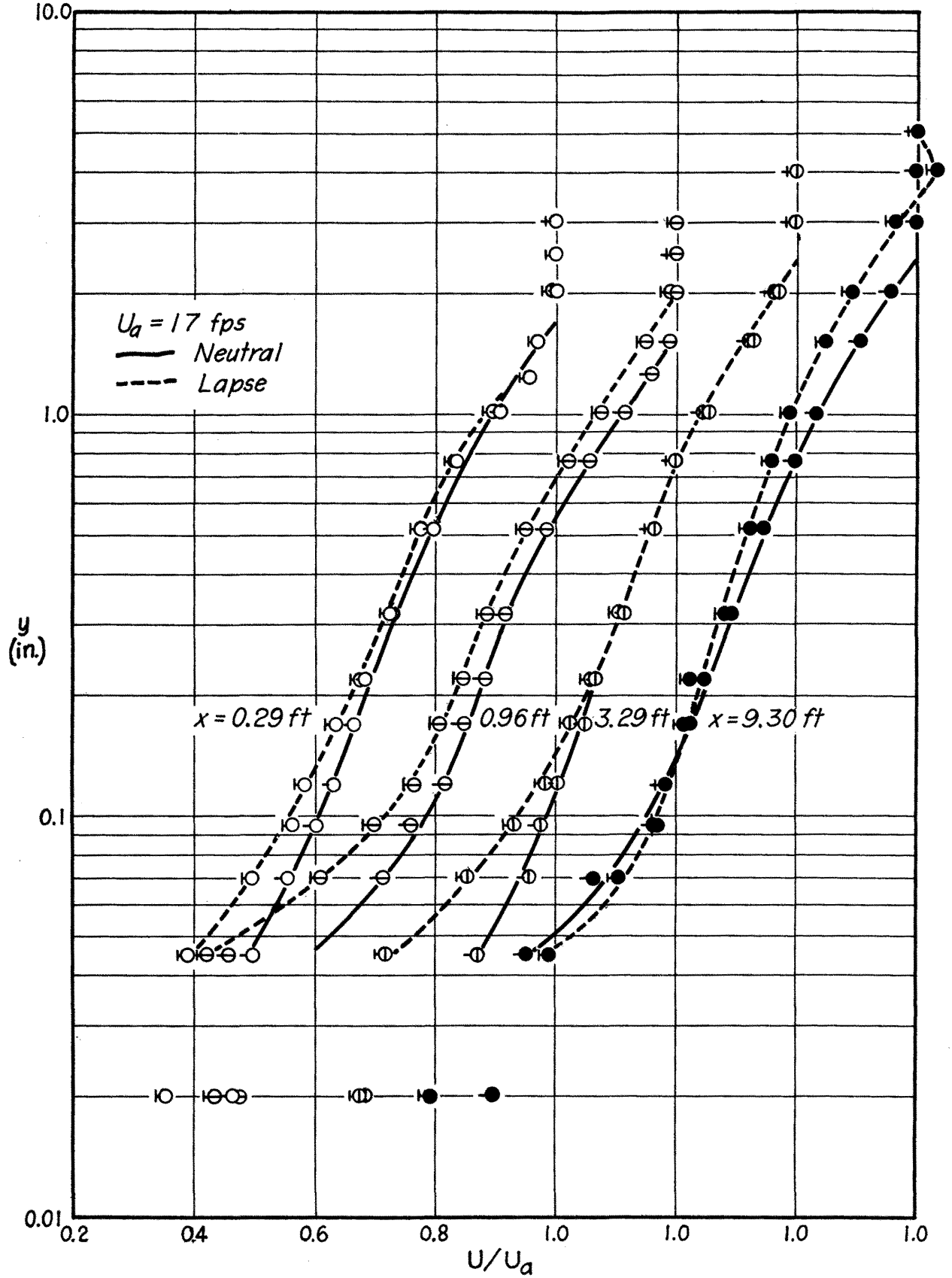

Fig. 13 Variation of U_N and U_L for U_a = 17 fps

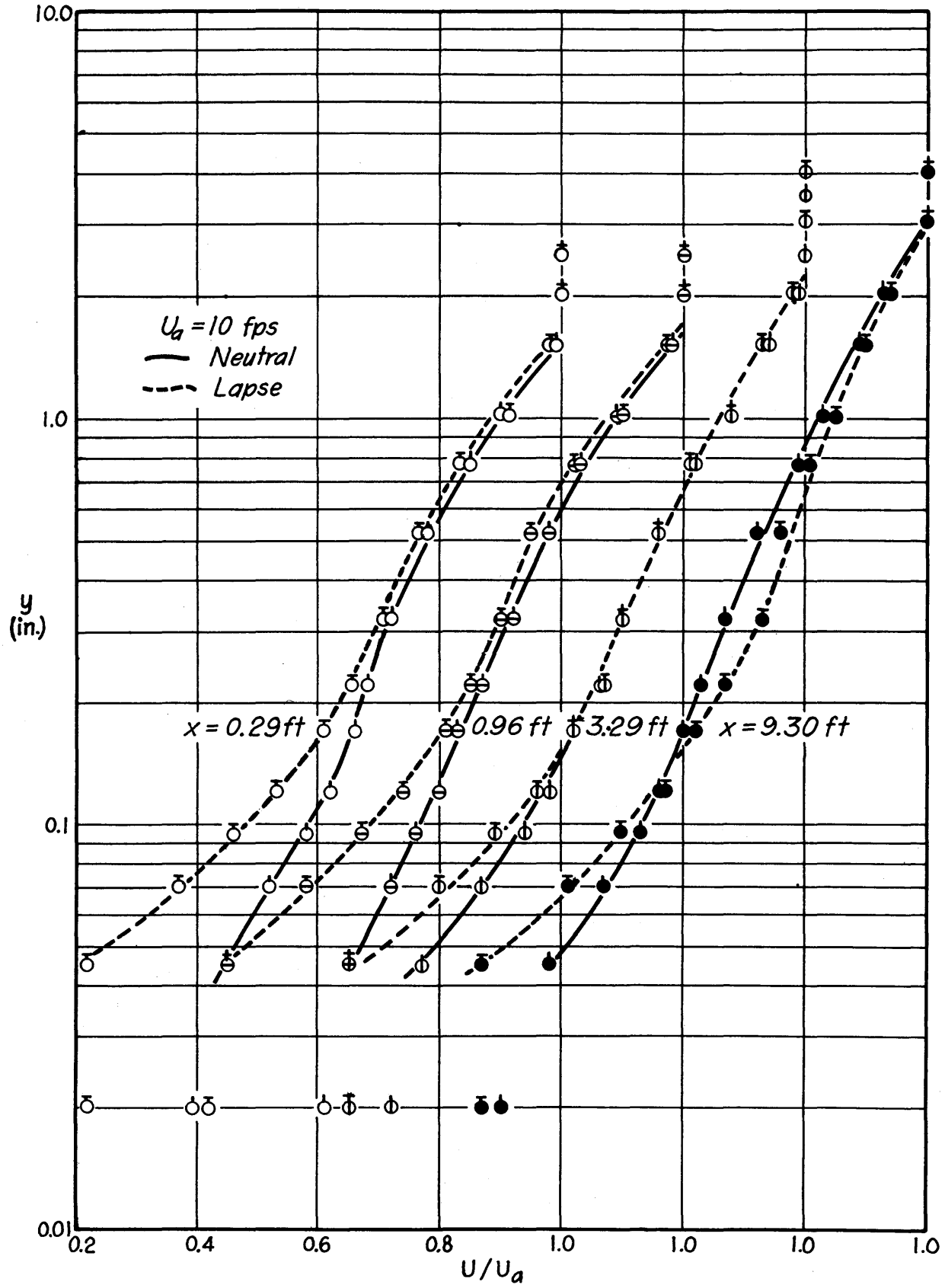

Fig. 14 Variation of U_N and U_L for U_a = 10 fps

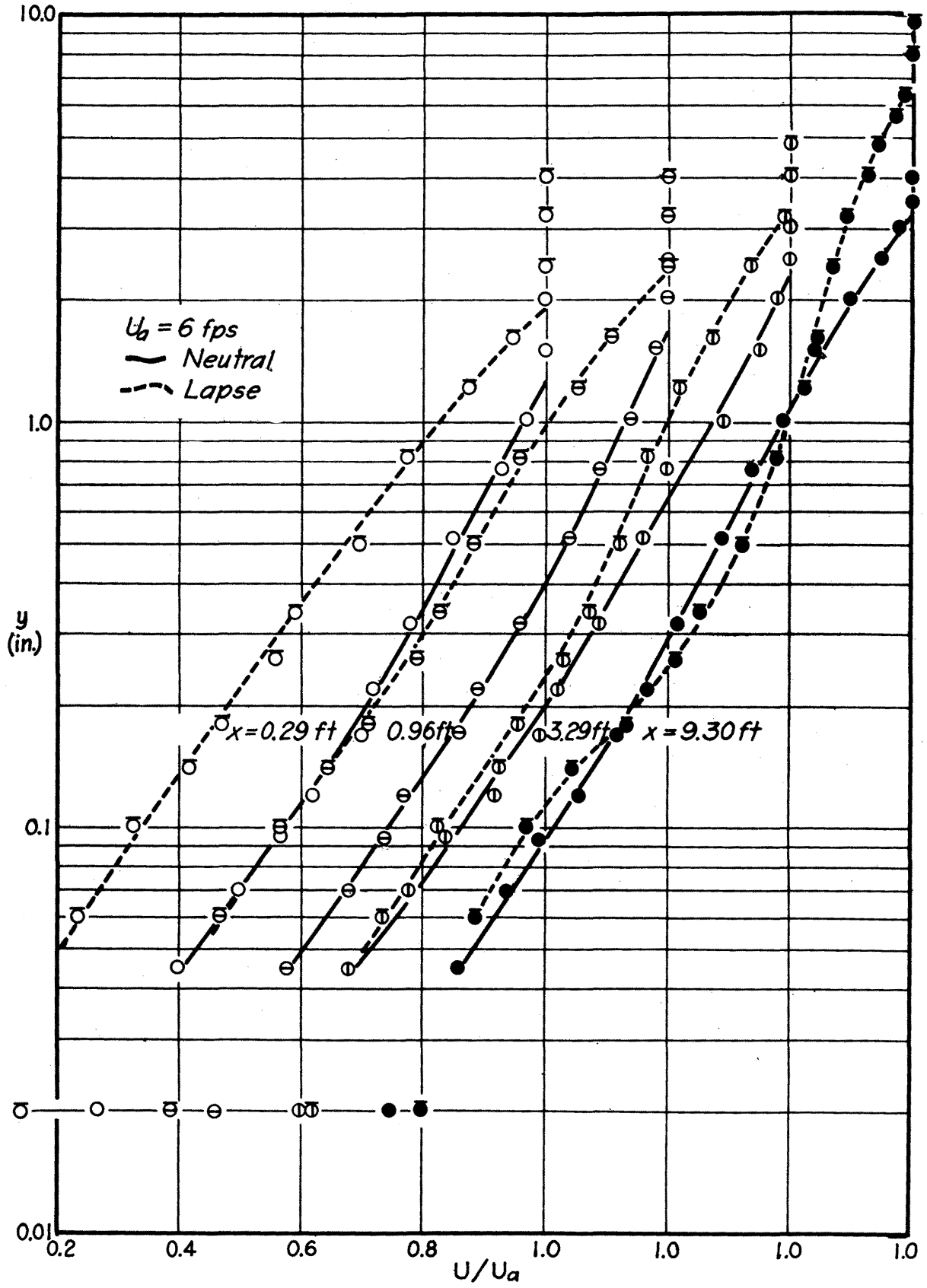

Fig. 15 Variation of U_N and U_L for U_a = 6 fps

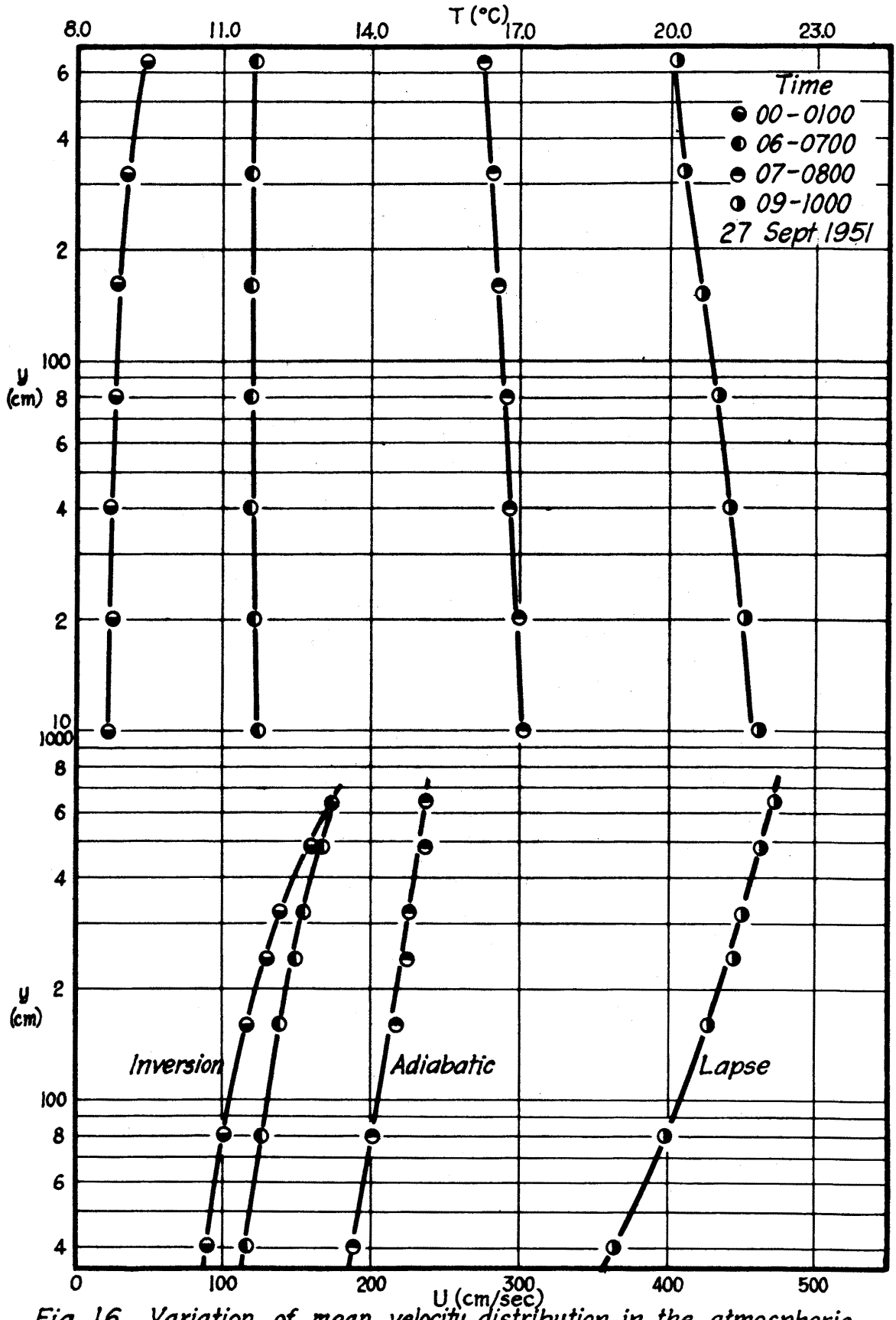

Fig. 16 Variation of mean velocity distribution in the atmospheric surface layer with stability — Halstead (3:48)

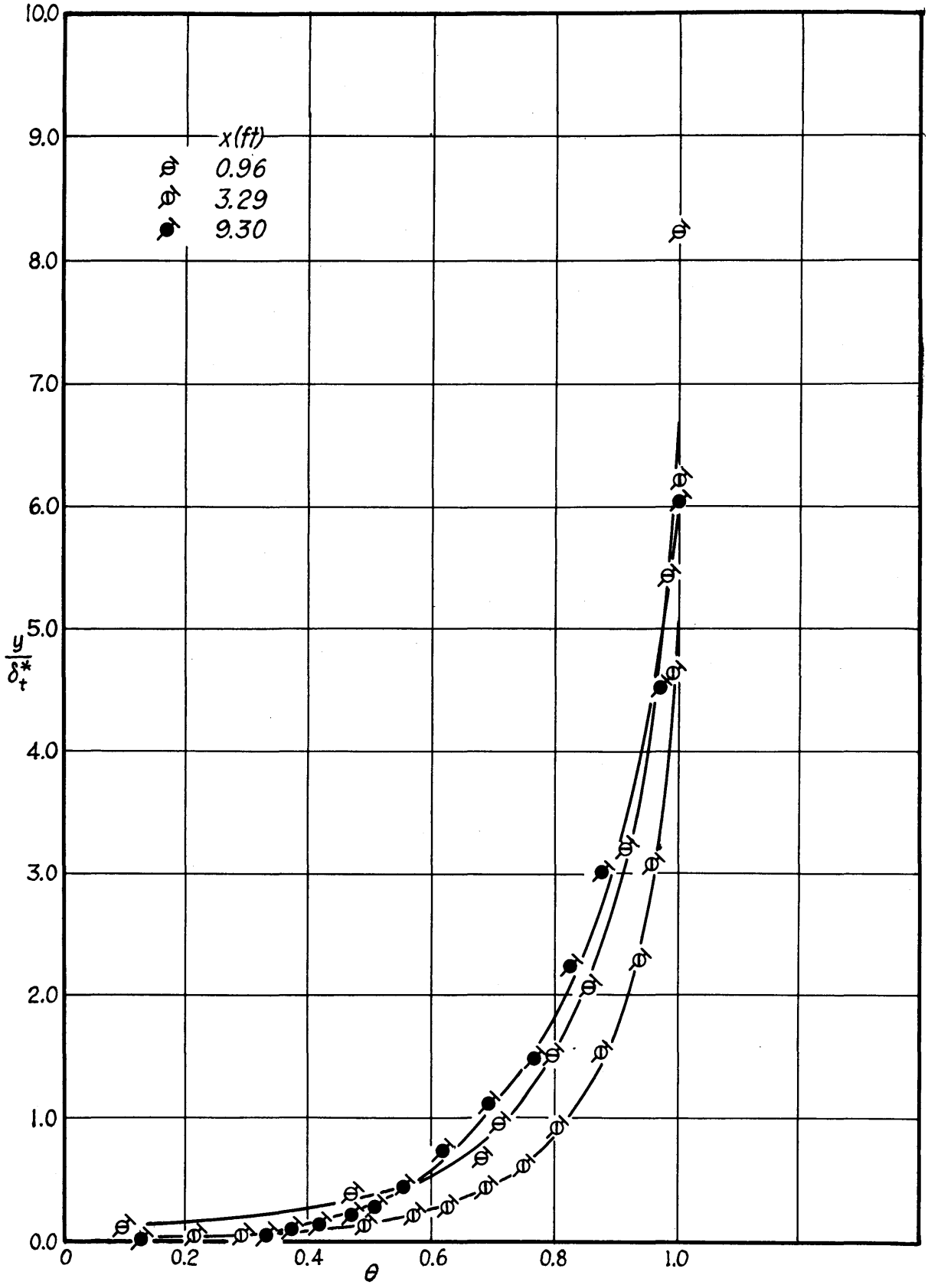

Fig. 17 Mean temperature distributions for $U_a = 35$ fps

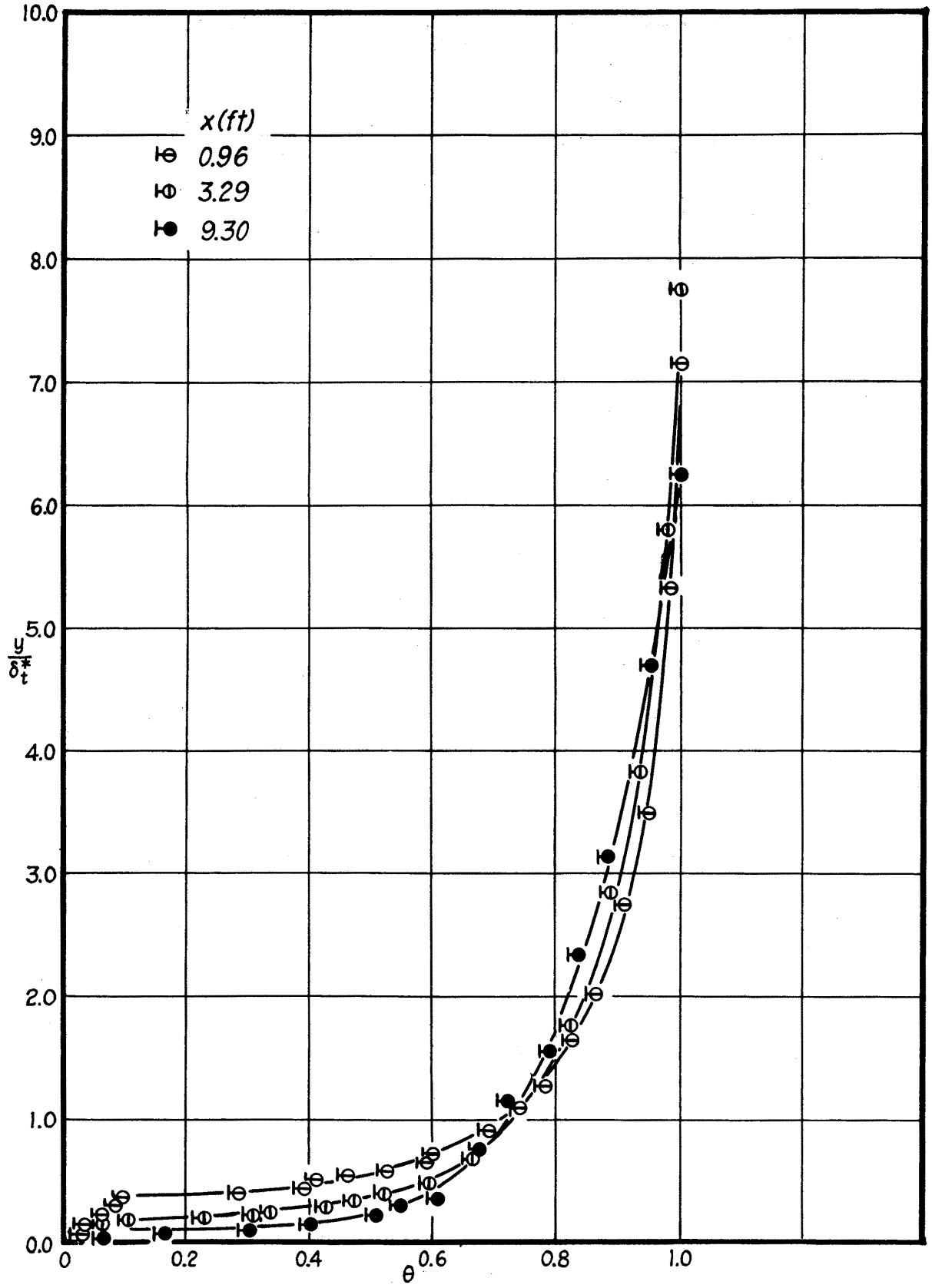

Fig. 18 Mean temperature distributions for $U_a = 17$ fps

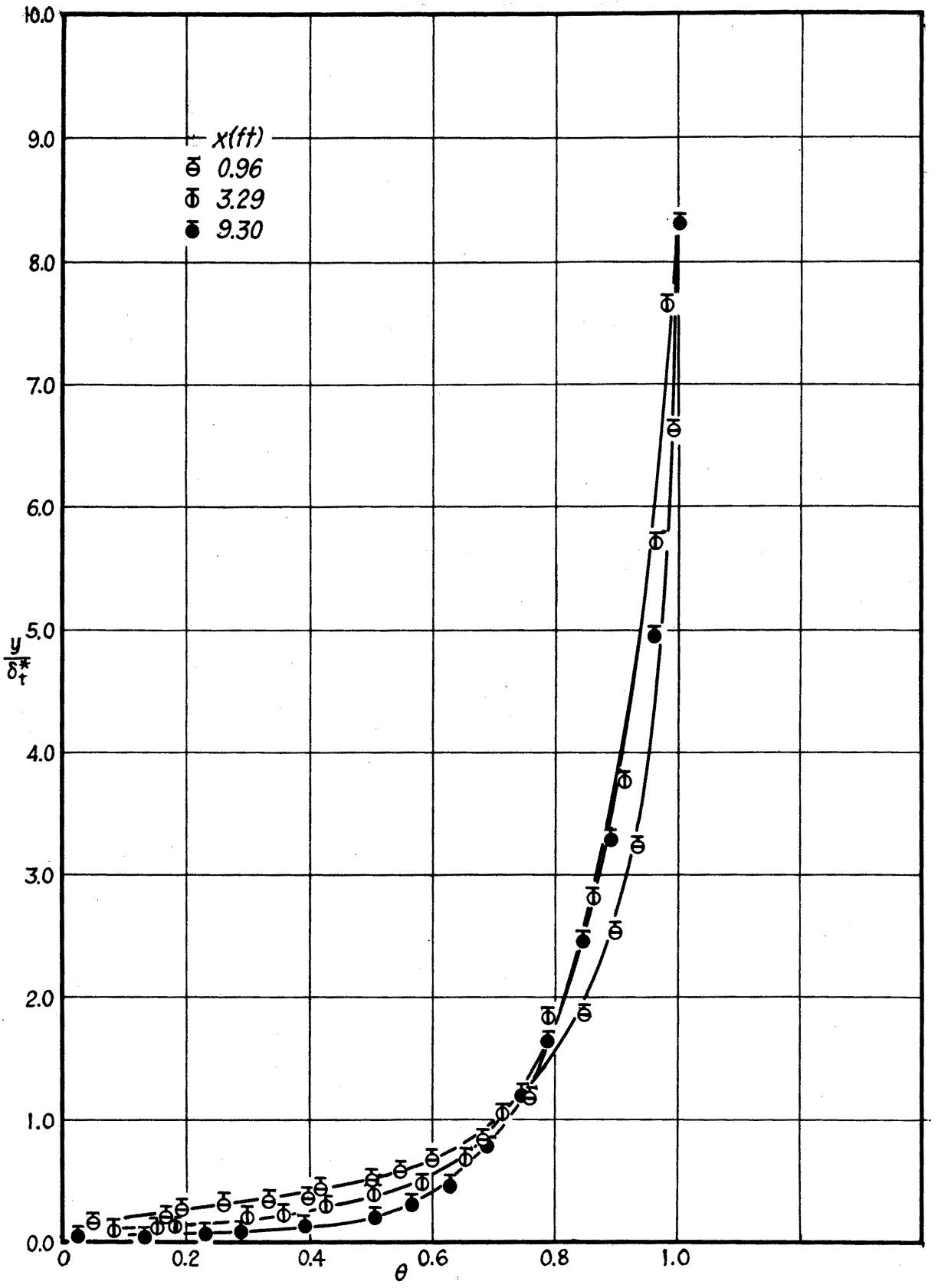

Fig. 19 Mean temperature distributions for $U_a = 10$ fps

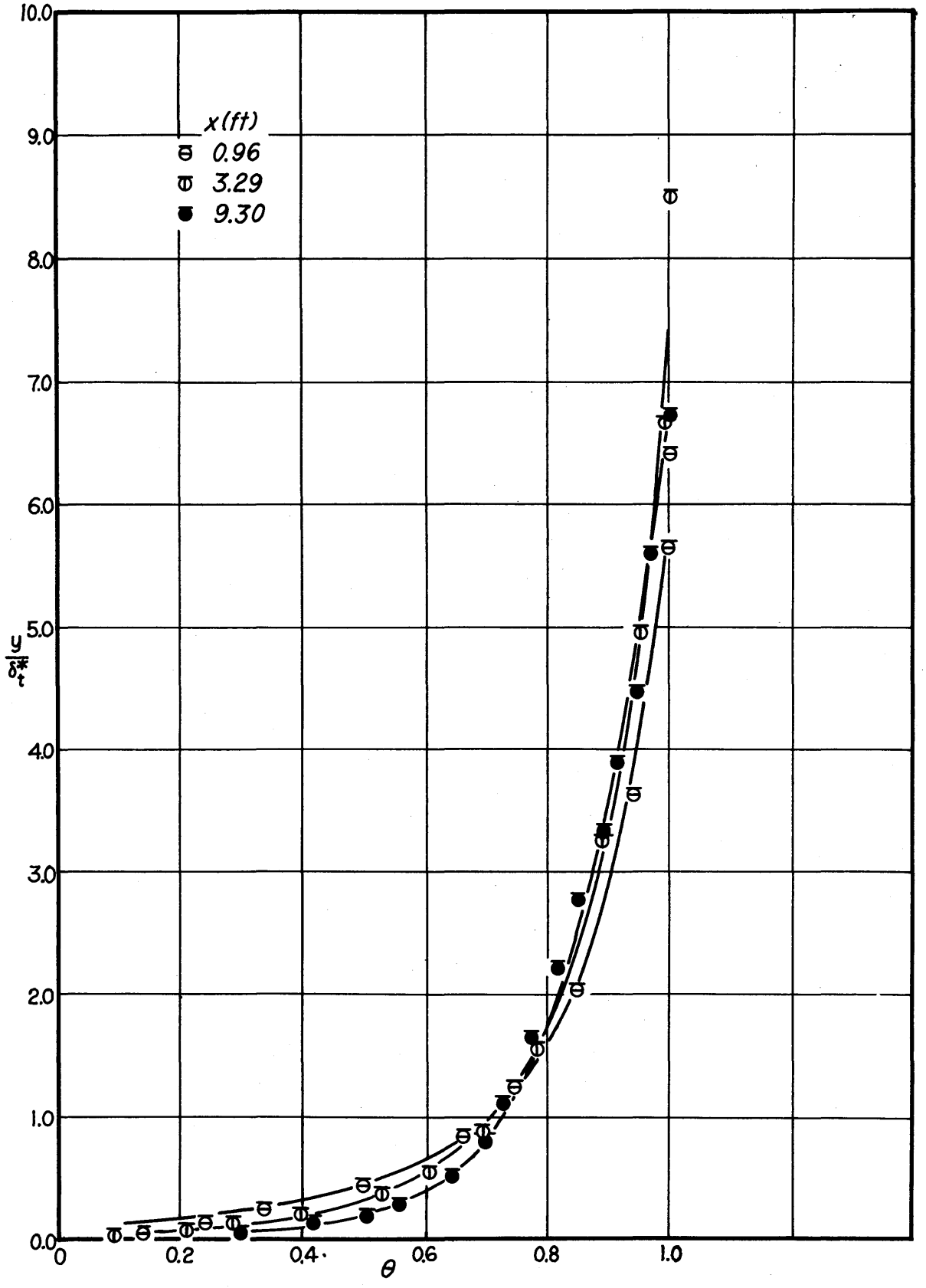

Fig. 20 Mean temperature distributions for U_a = 6 fps

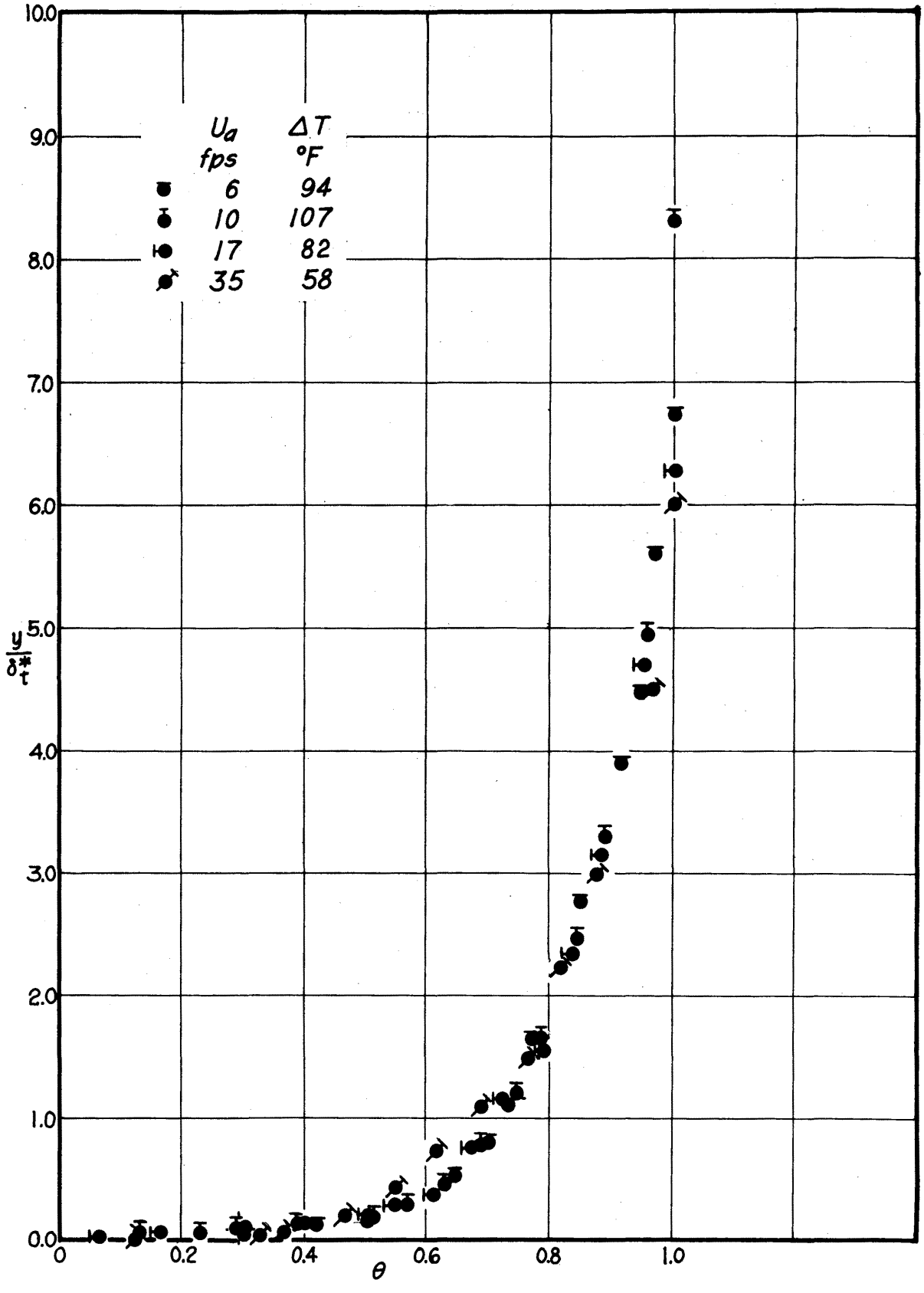

Fig. 21 Comparison of mean temperature distributions for x=9.30 ft

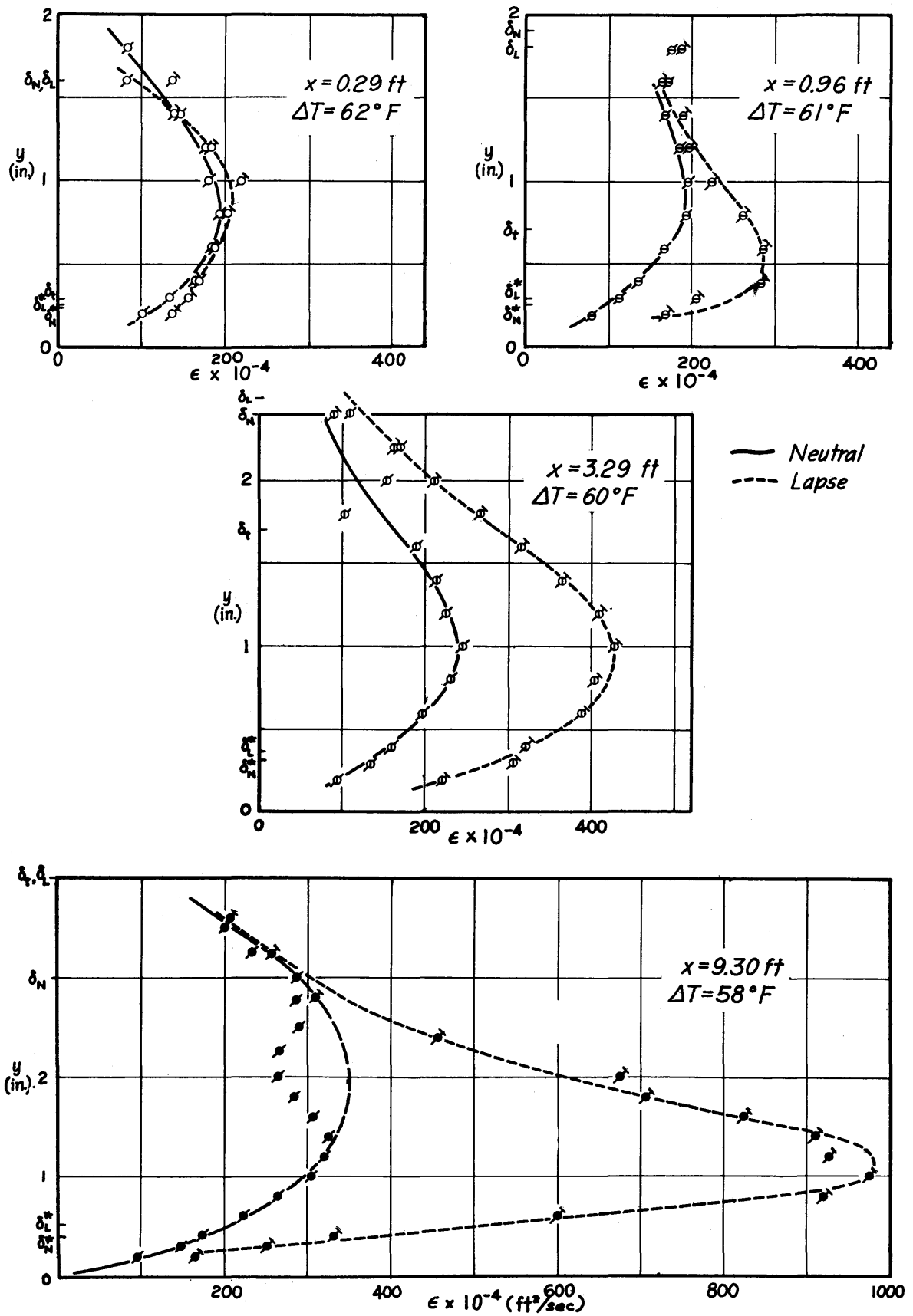

Fig. 22 Variation of ϵ_N and ϵ_L for $U_a = 35$ fps

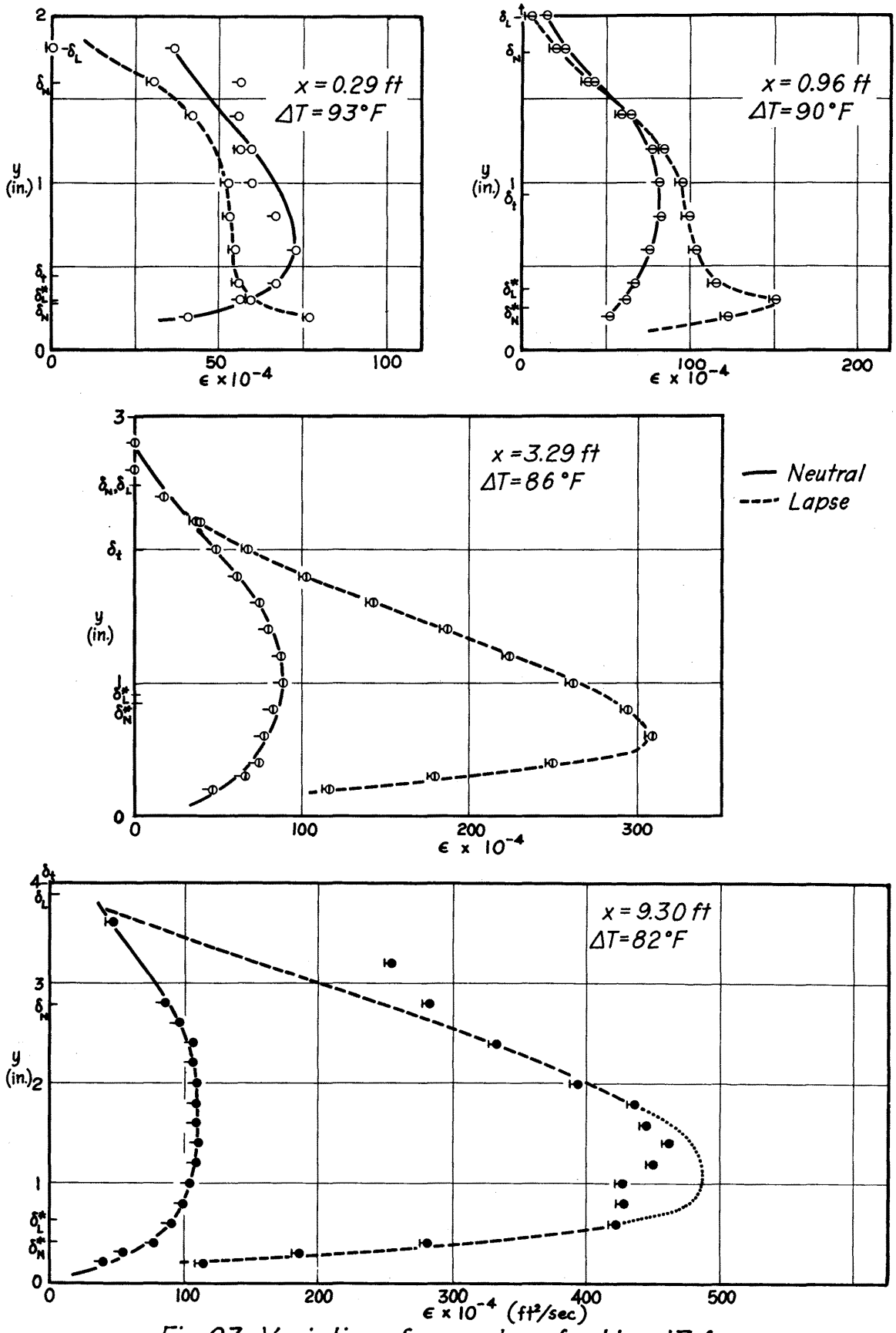

Fig. 23 Variation of ϵ_N and ϵ_L for U_a = 17 fps

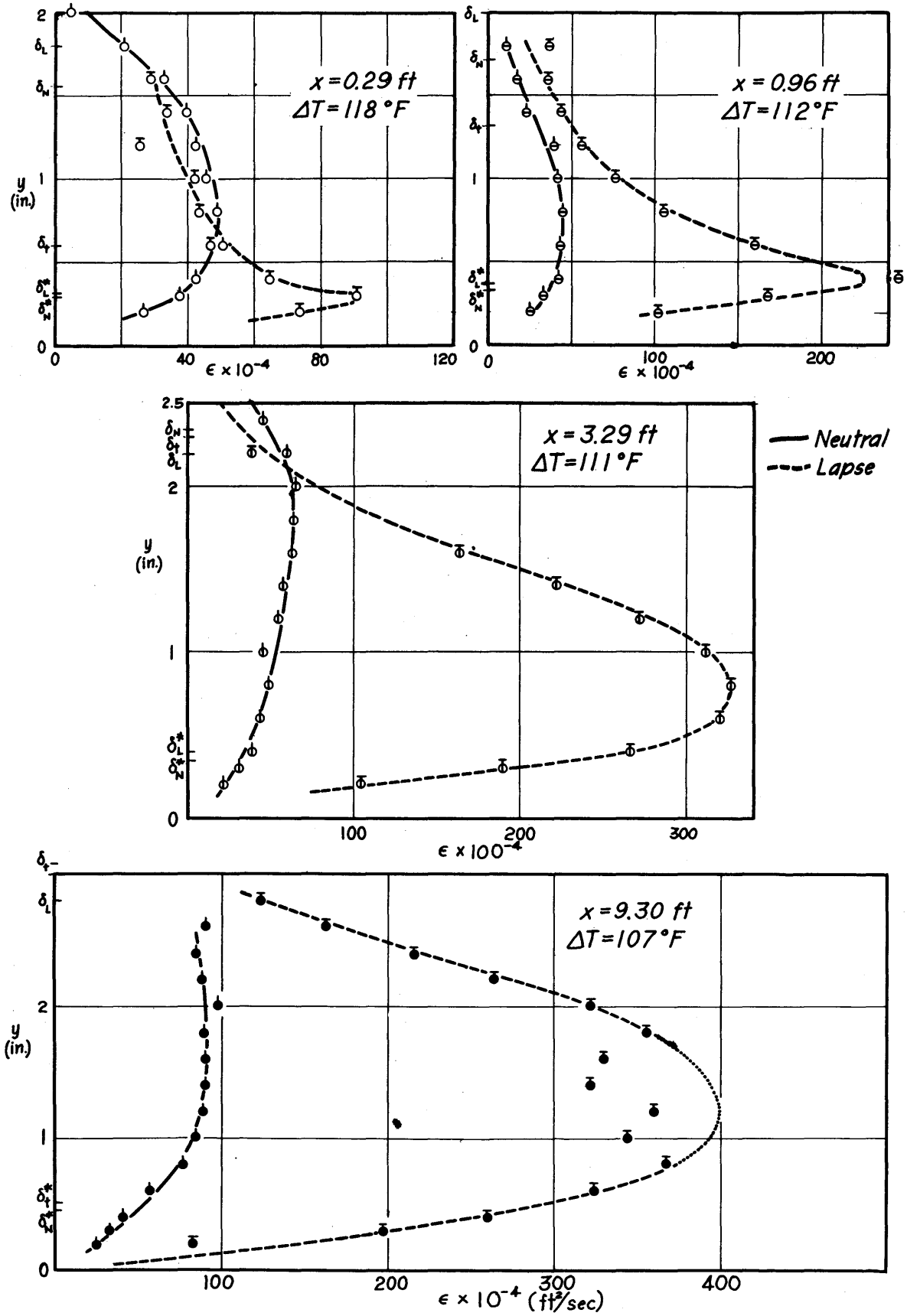

Fig. 24 Variation of ϵ_N and ϵ_L for U_a = 10 fps

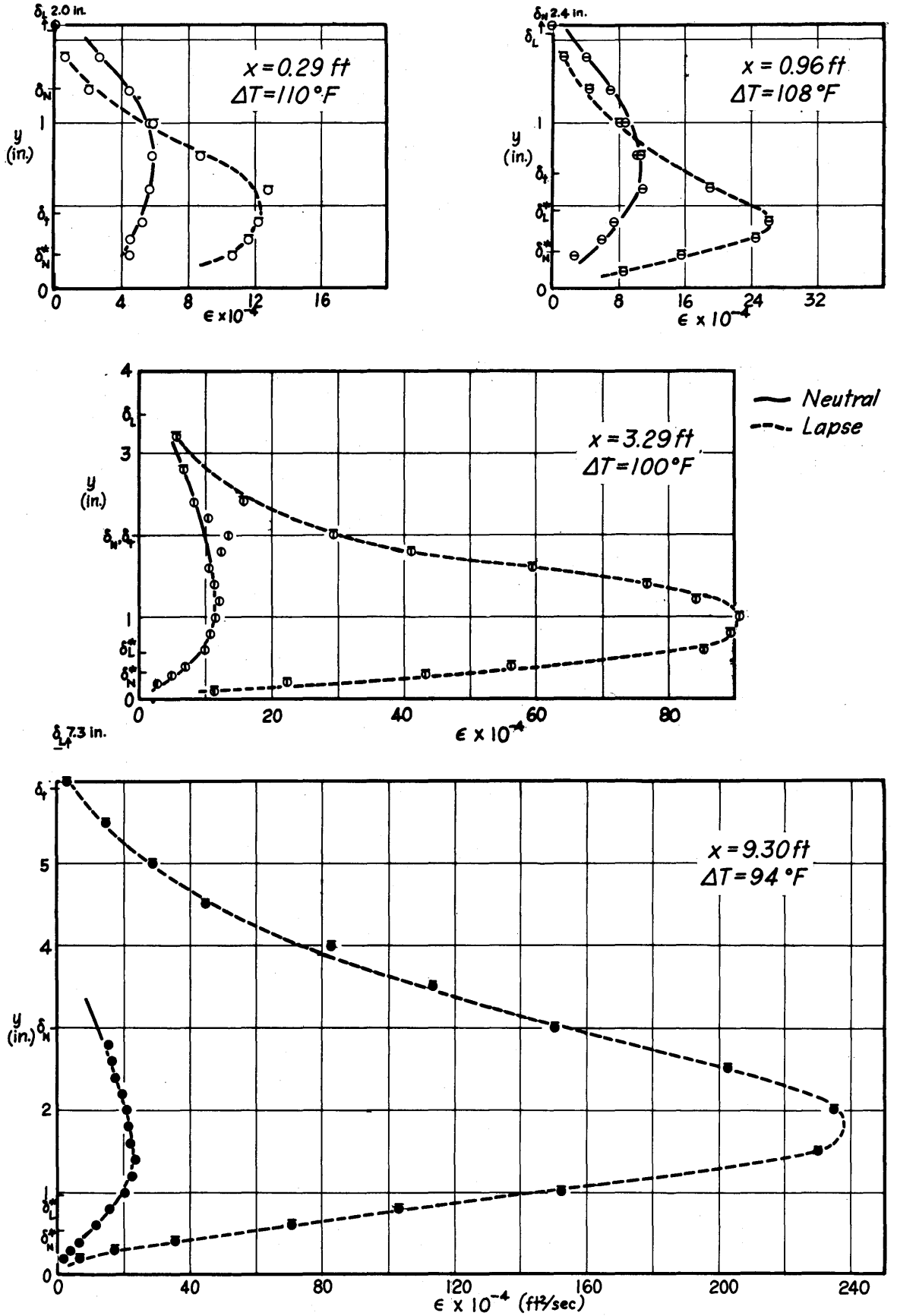

Fig. 25 Variation of ϵ_N and ϵ_L for $U_a = 6$ fps

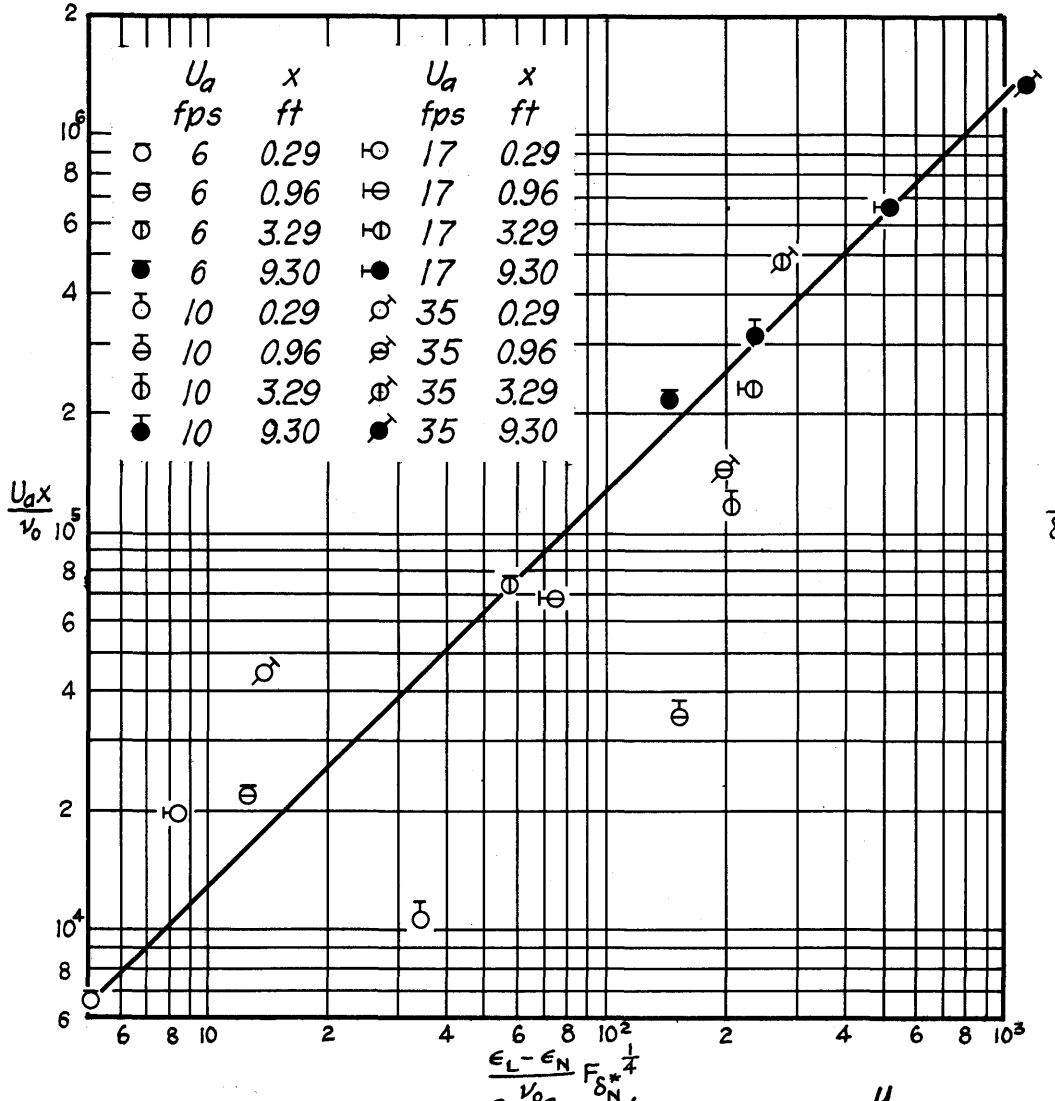

Fig. 26 Variation of $\frac{\epsilon_L - \epsilon_N}{\nu_0} F_{\delta_N^*}^{\frac{1}{4}}$ with R_x for $\frac{y}{\delta_N^*} = 3$

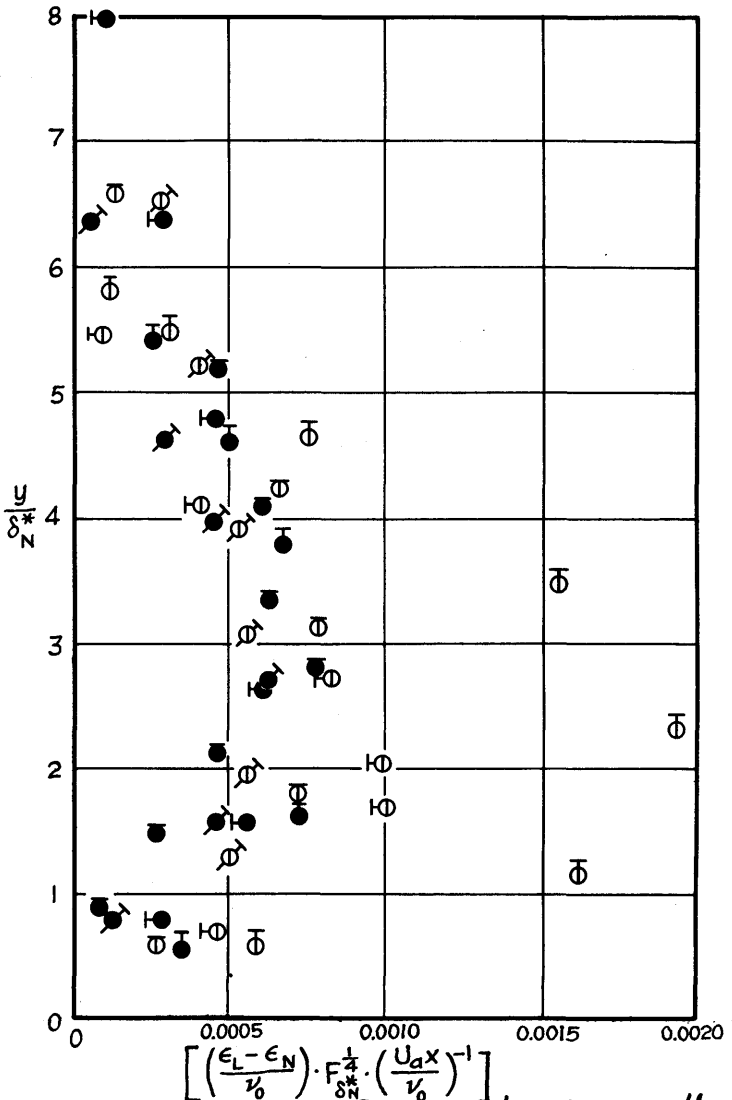

Fig. 27 Variation of $\frac{\epsilon_L - \epsilon_N}{\nu_0} F_{\delta_N^*}^{\frac{1}{4}} R_x^{-1}$ with $\frac{y}{\delta_N^*}$

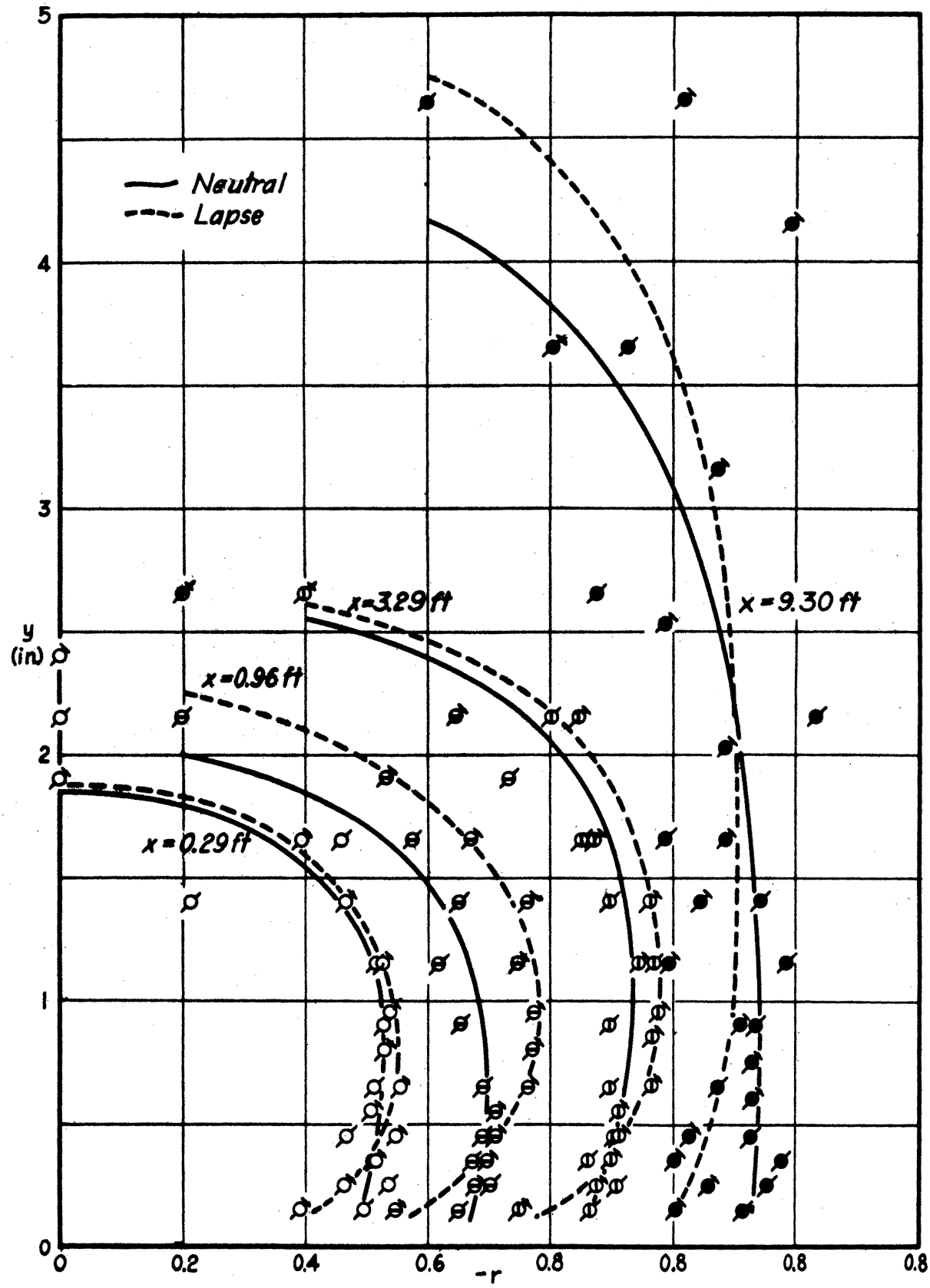

Fig. 28 Variation of r_N and r_L for $U_0 = 35$ fps

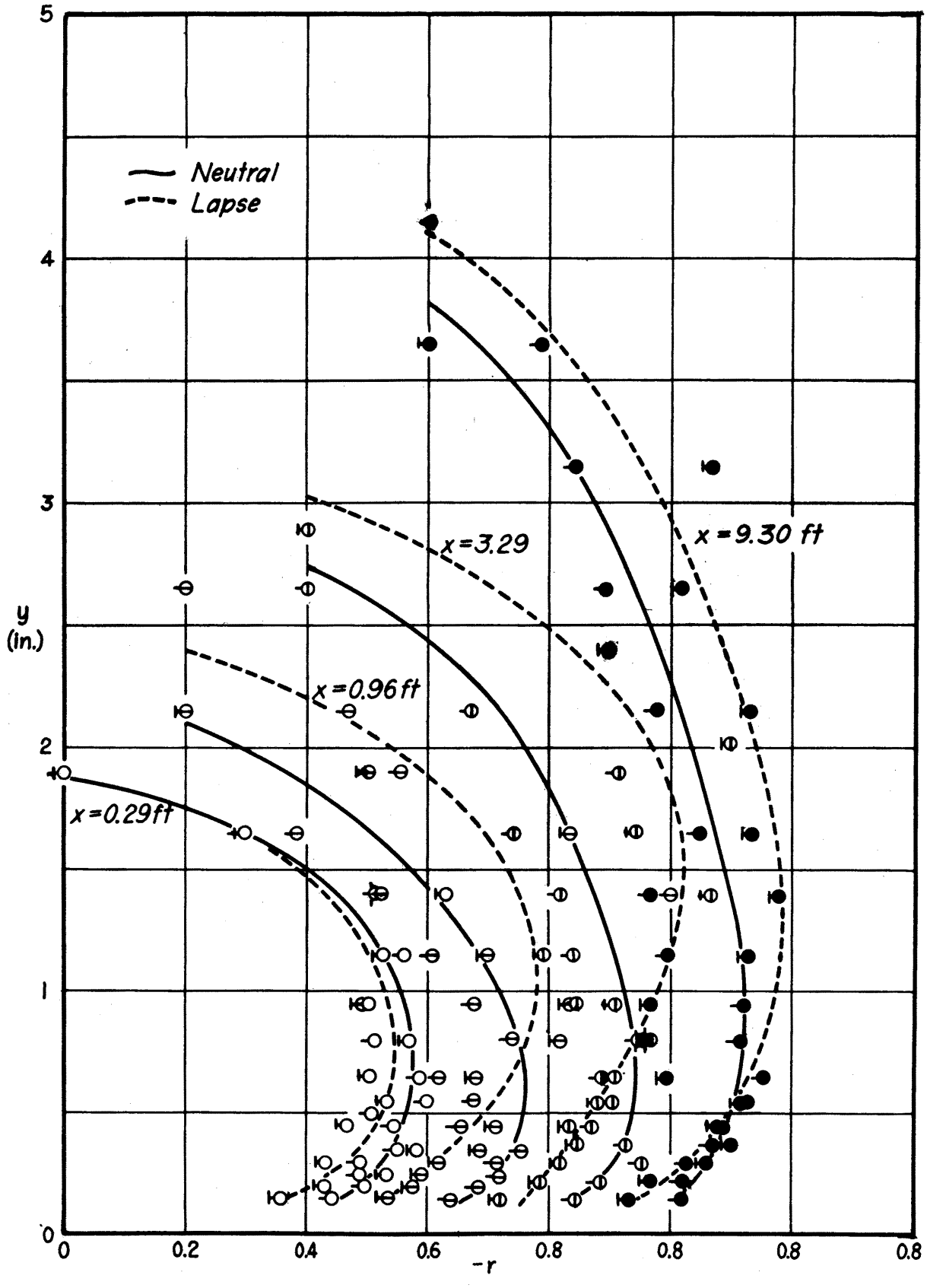

Fig. 29 Variation of r_N and r_L for $U_a = 17$ fps

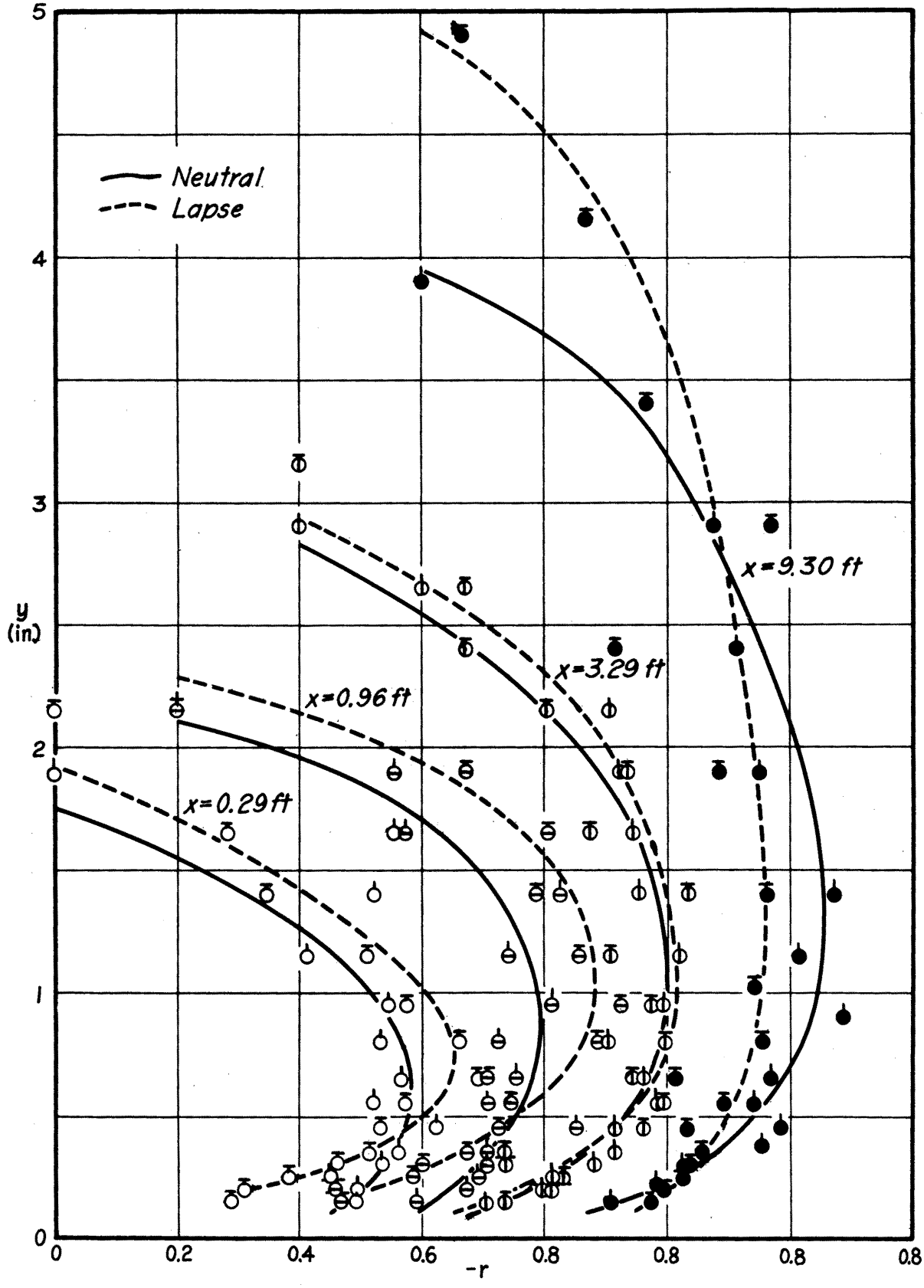

Fig. 30 Variation of r_N and r_L for $U_a = 10$ fps

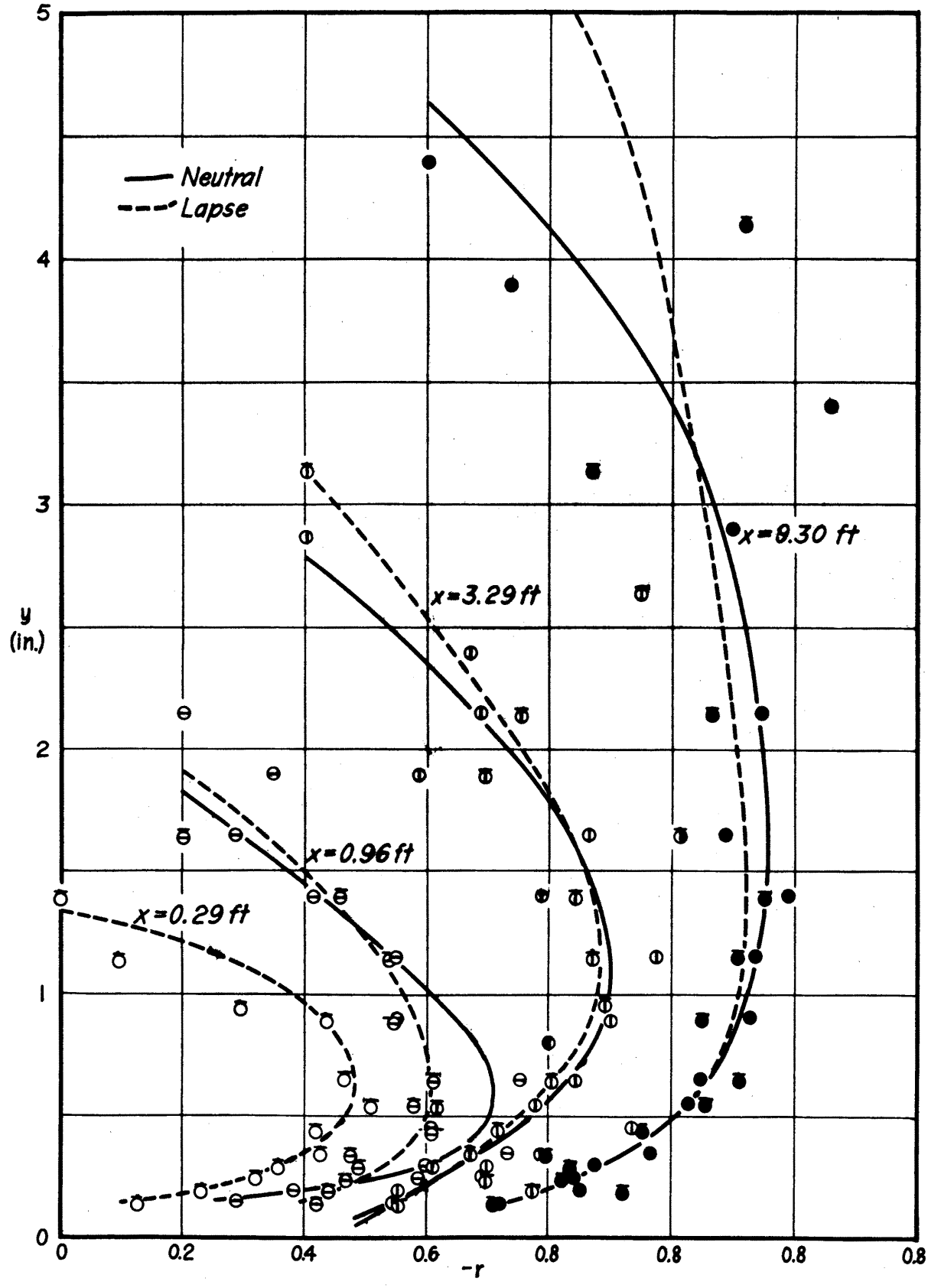

Fig. 31 Variation of r_N and r_L for $U_a = 6$ fps

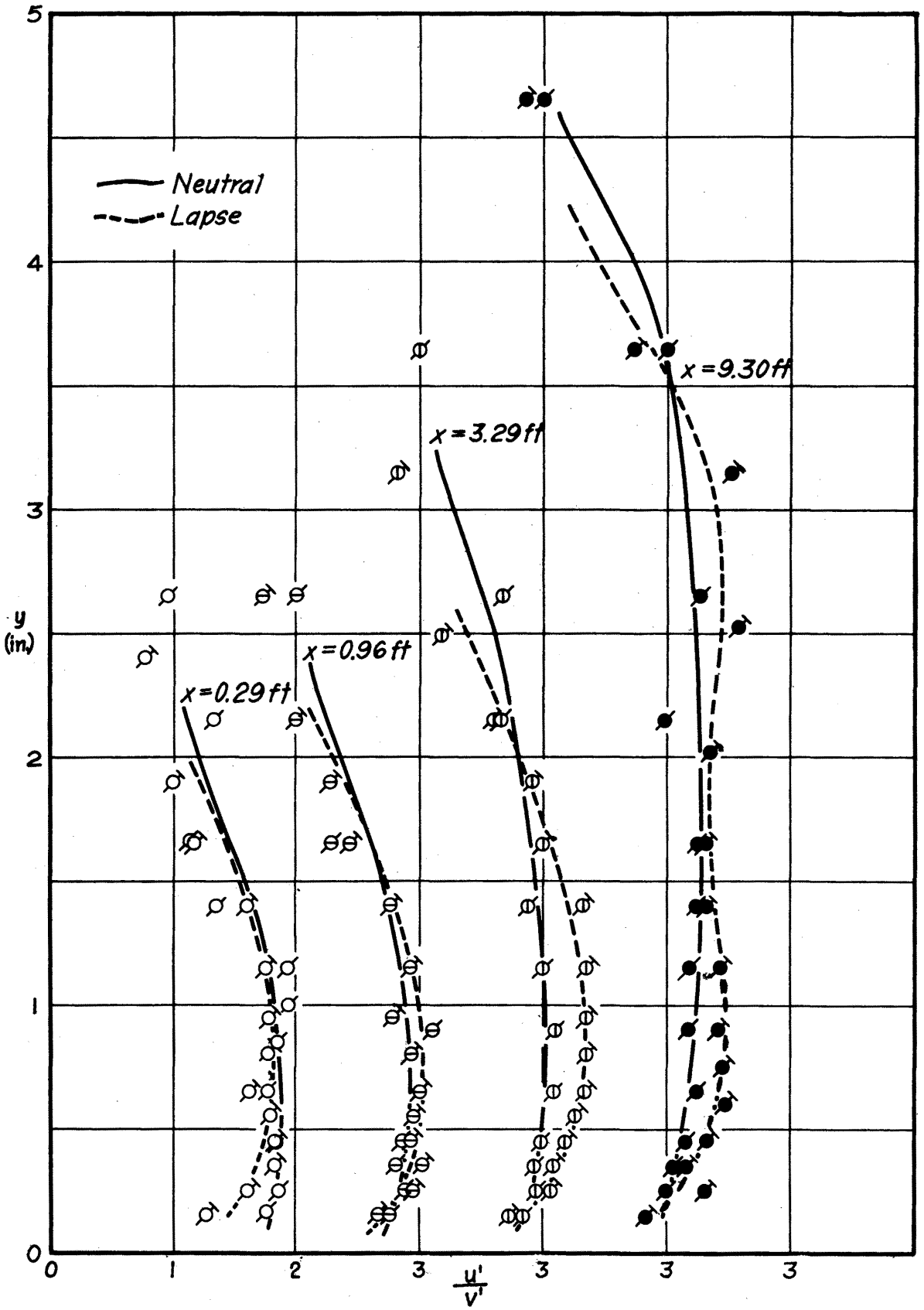

Fig. 32 Variation of $\left(\frac{u'}{v'}\right)_N$ and $\left(\frac{u'}{v'}\right)_L$ for $U_a = 35$ fps

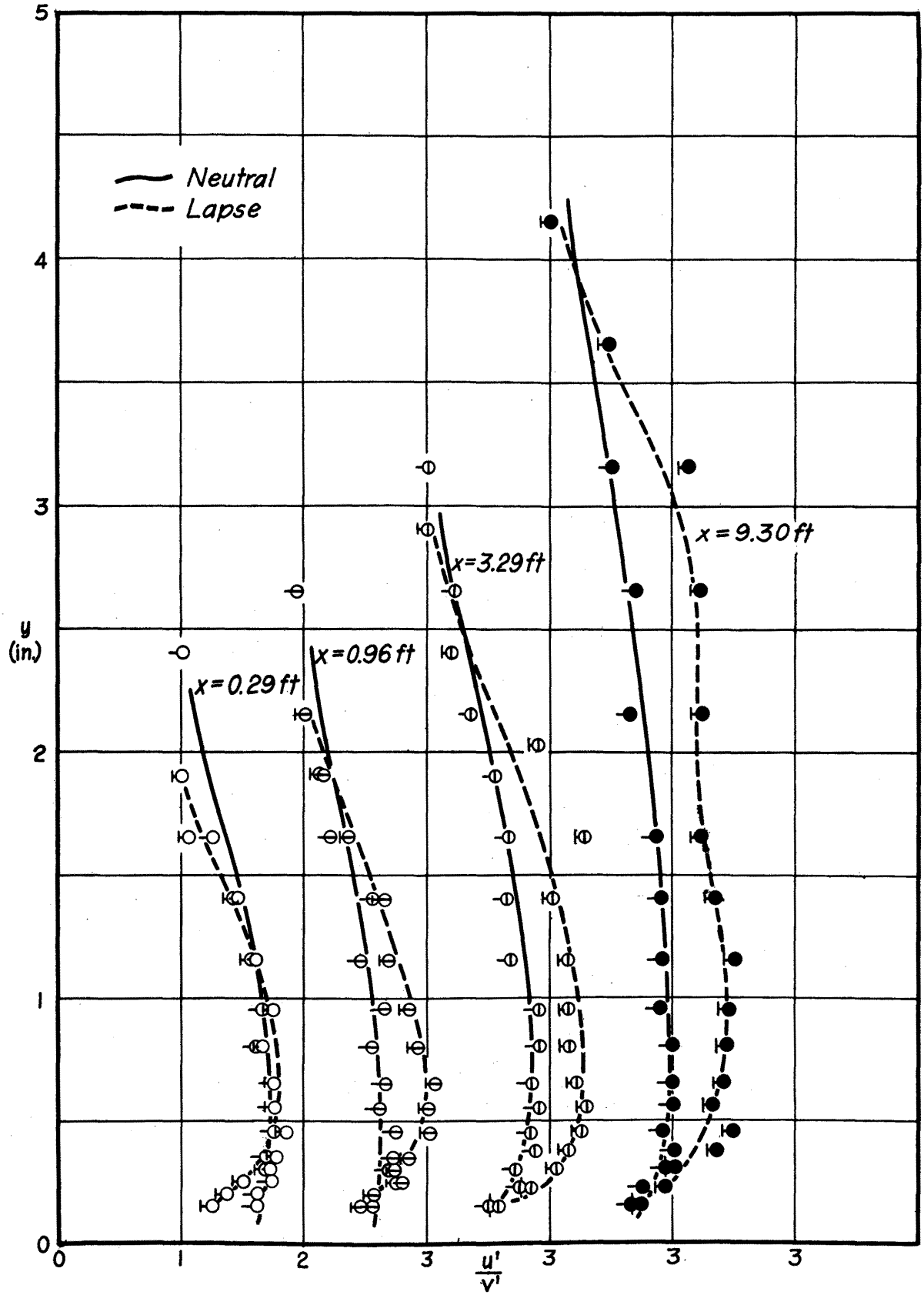

Fig. 33 Variation of $\left(\frac{u'}{v'}\right)_N$ and $\left(\frac{u'}{v'}\right)_L$ for $U_a = 17$ fps

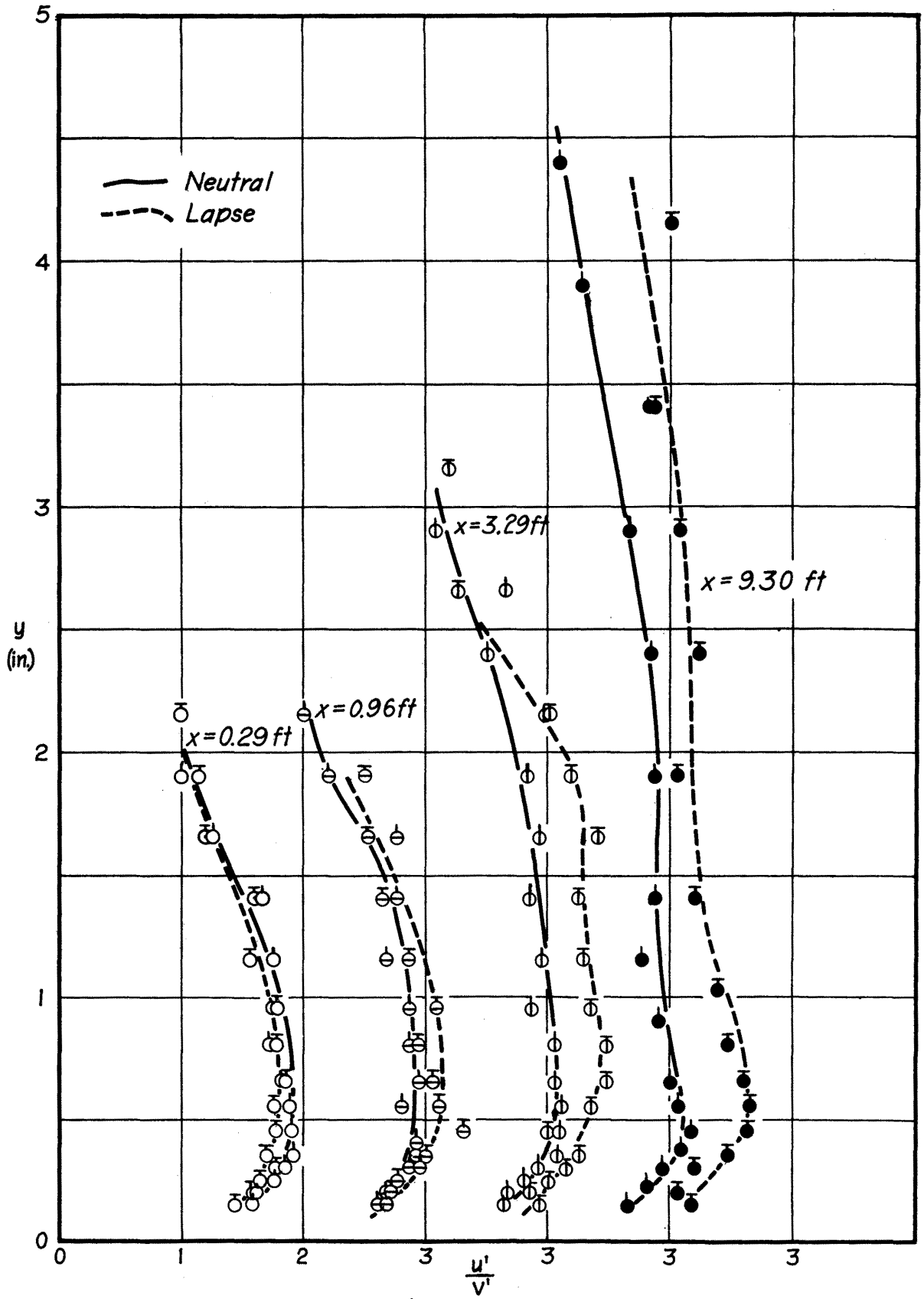

Fig. 34 Variation of $\left(\frac{u'}{v'}\right)_N$ and $\left(\frac{u'}{v'}\right)_L$ for $U_a = 10$ fps

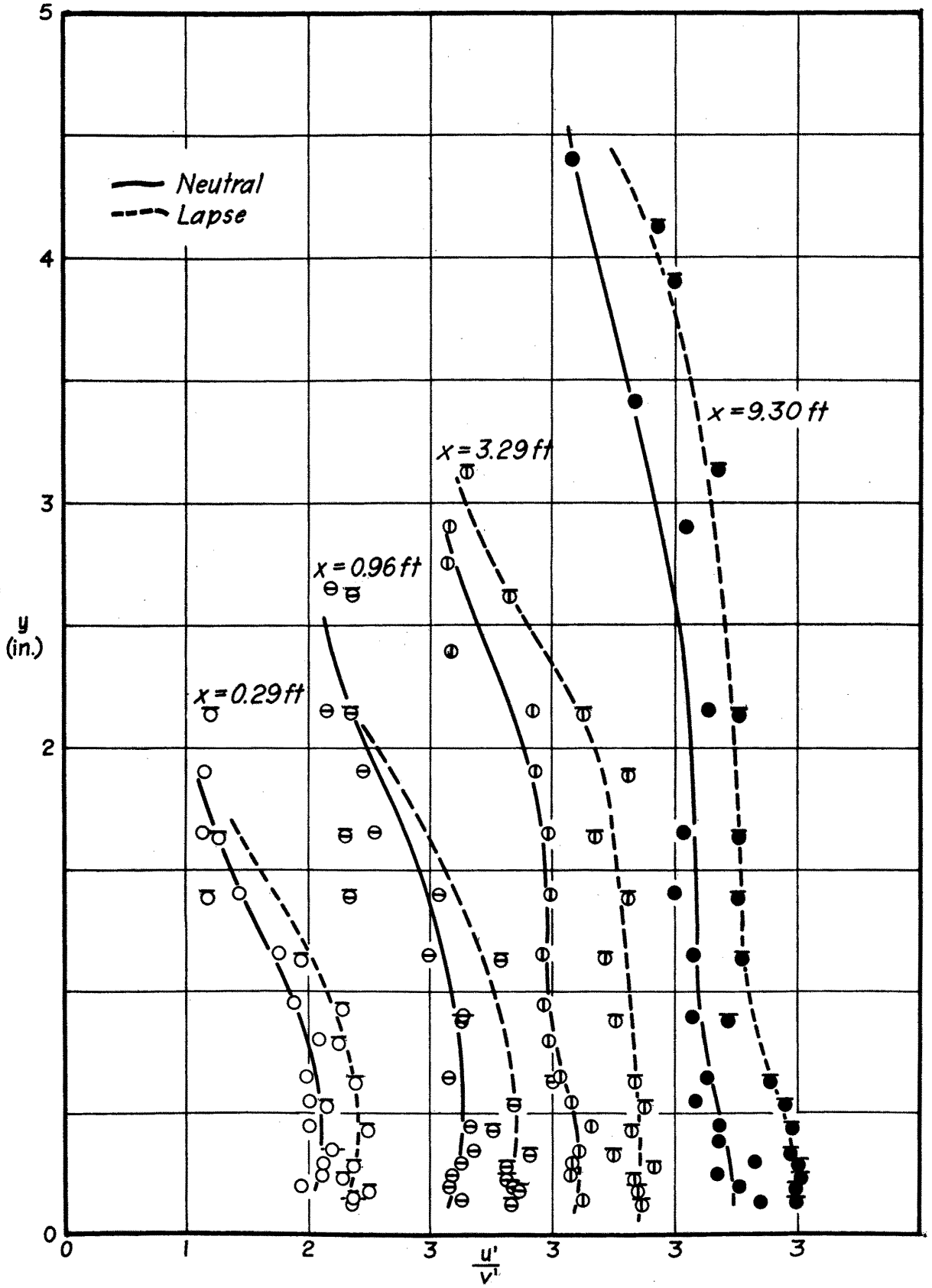

Fig. 35 Variation of $\left(\frac{u'}{v'}\right)_N$ and $\left(\frac{u'}{v'}\right)_L$ for $U_a = 6$ fps

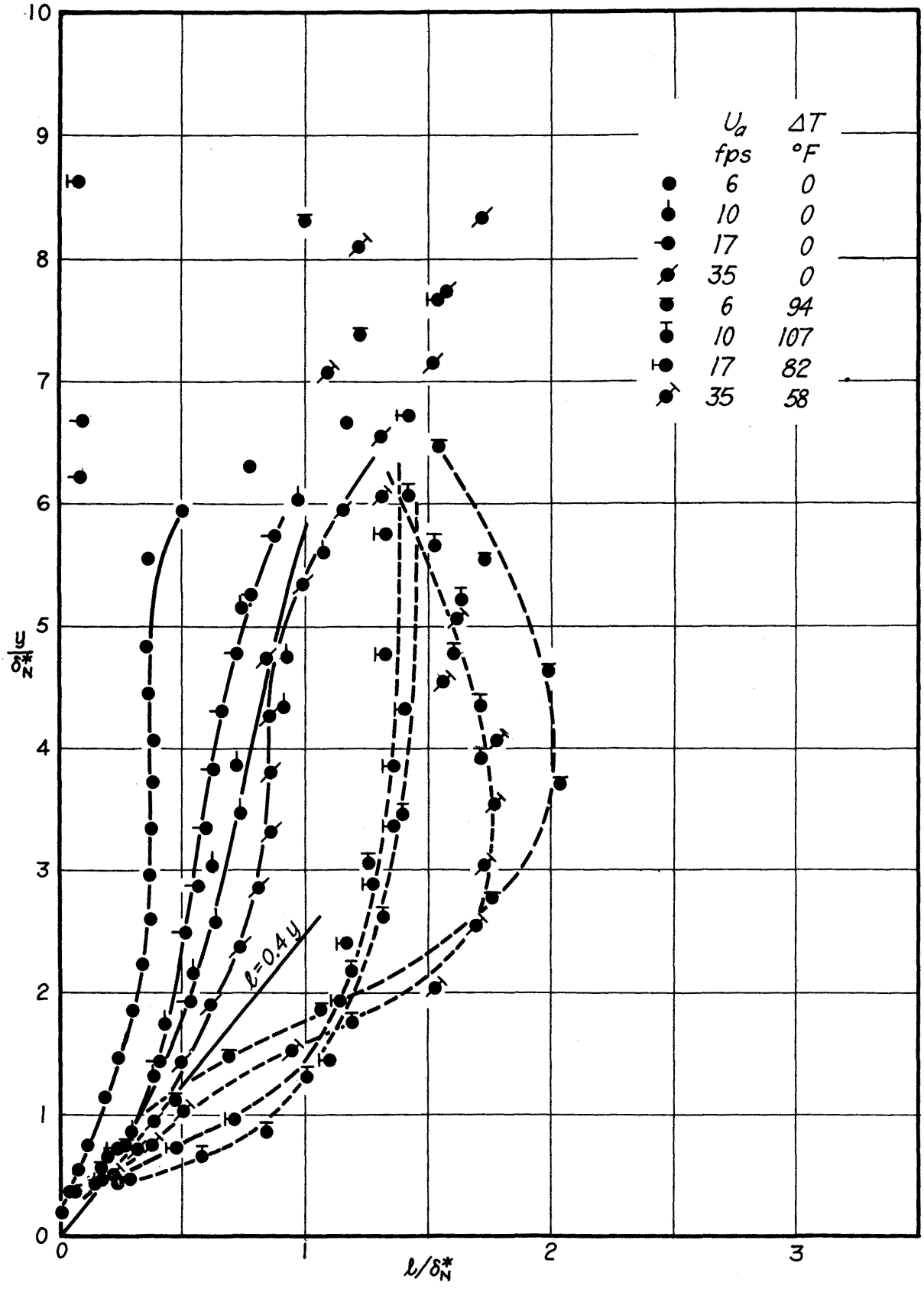

Fig. 36 Variation of $\left(\frac{l}{\delta_N^*}\right)_N$ and $\left(\frac{l}{\delta_N^*}\right)_L$ for $x = 9.30$ ft

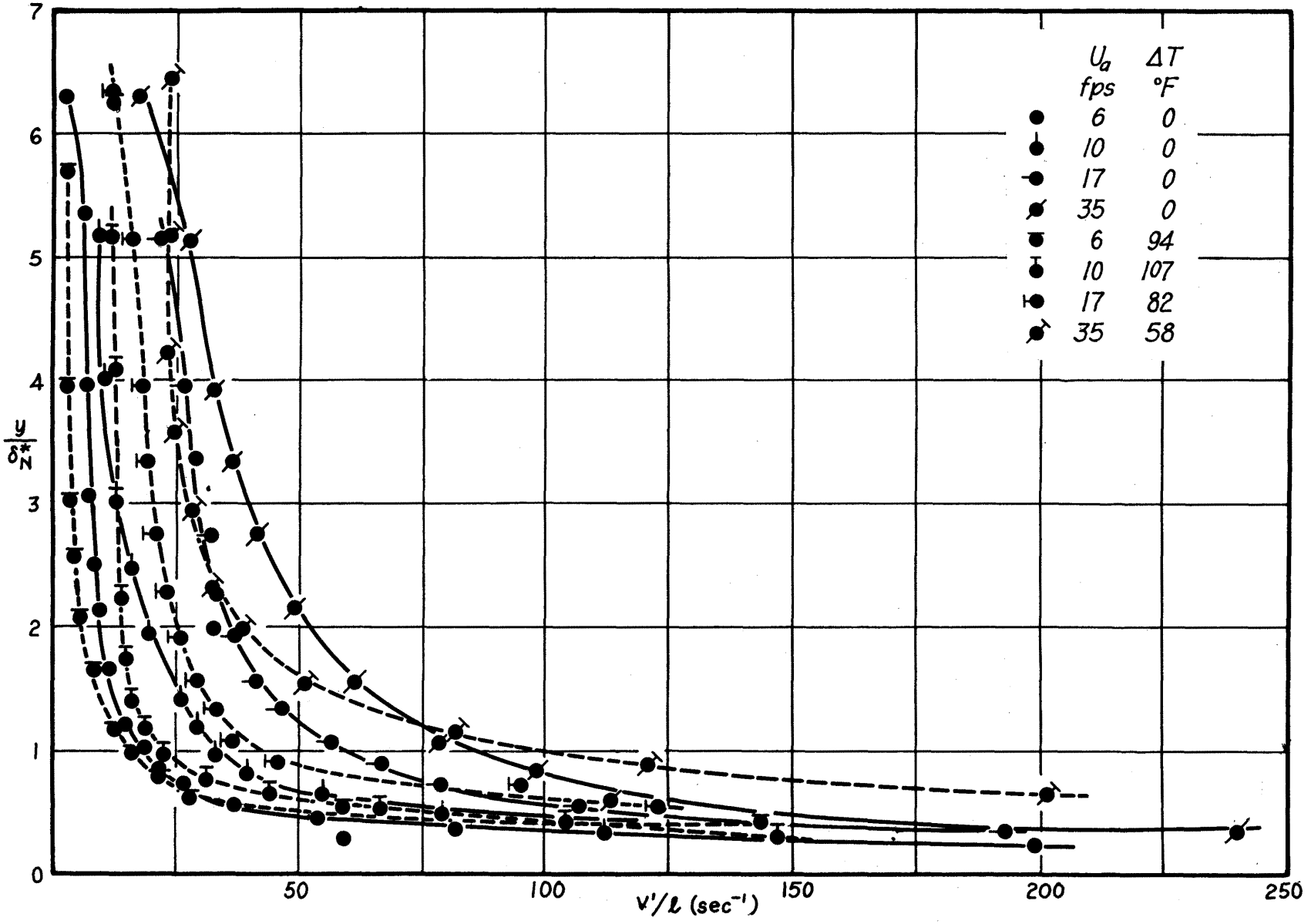

Fig. 37 Variation of $\left(\frac{V'}{\ell}\right)_N$ and $\left(\frac{V'}{\ell}\right)_L$ for $x = 9.30$ ft

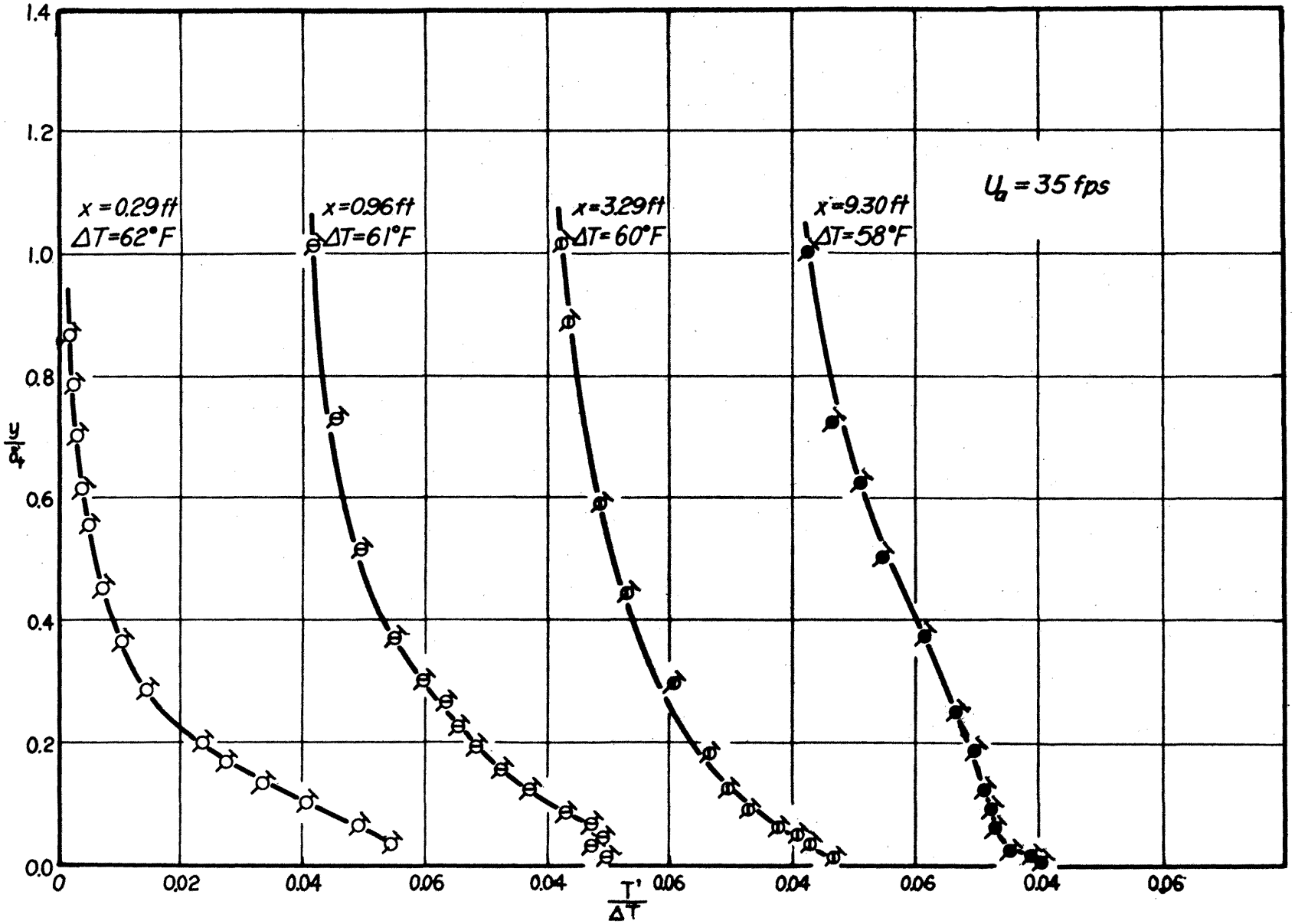

Fig. 38 Distribution of temperature fluctuation intensity for $U_0 = 35$ fps

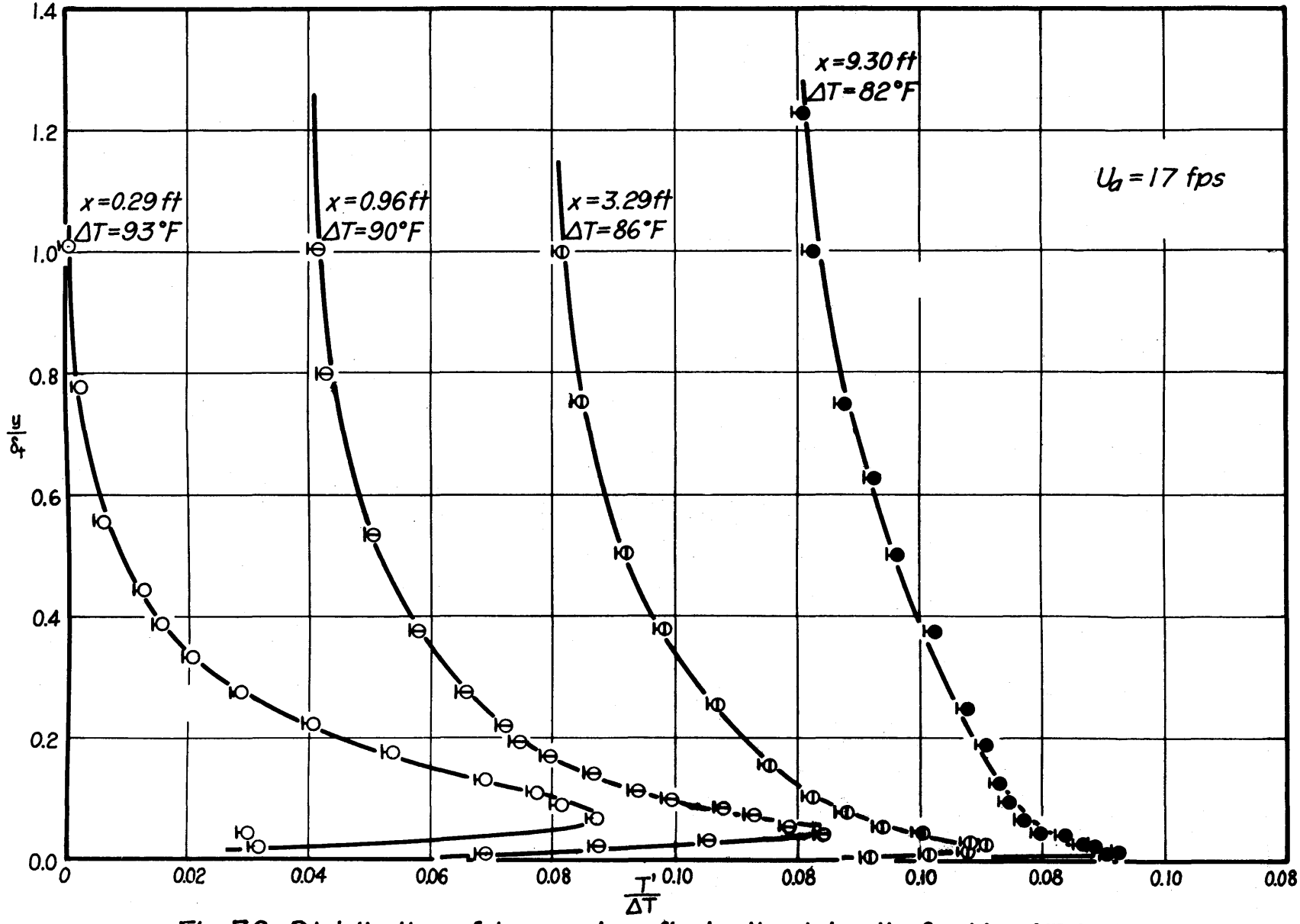

Fig. 39 Distribution of temperature fluctuation intensity for U_a = 17 fps

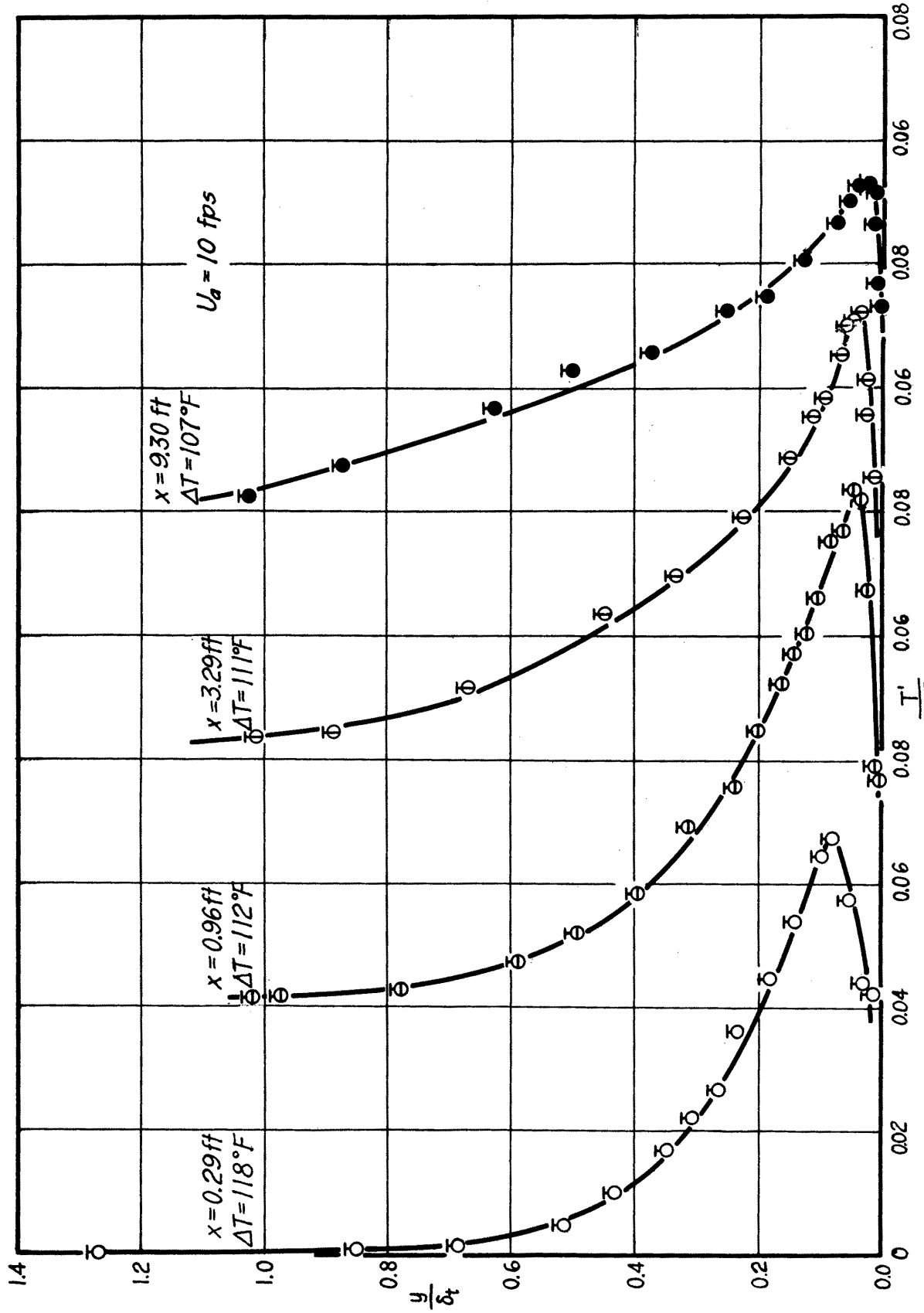

Fig. 40 Distribution of temperature fluctuation intensity for U_a = 10 fps

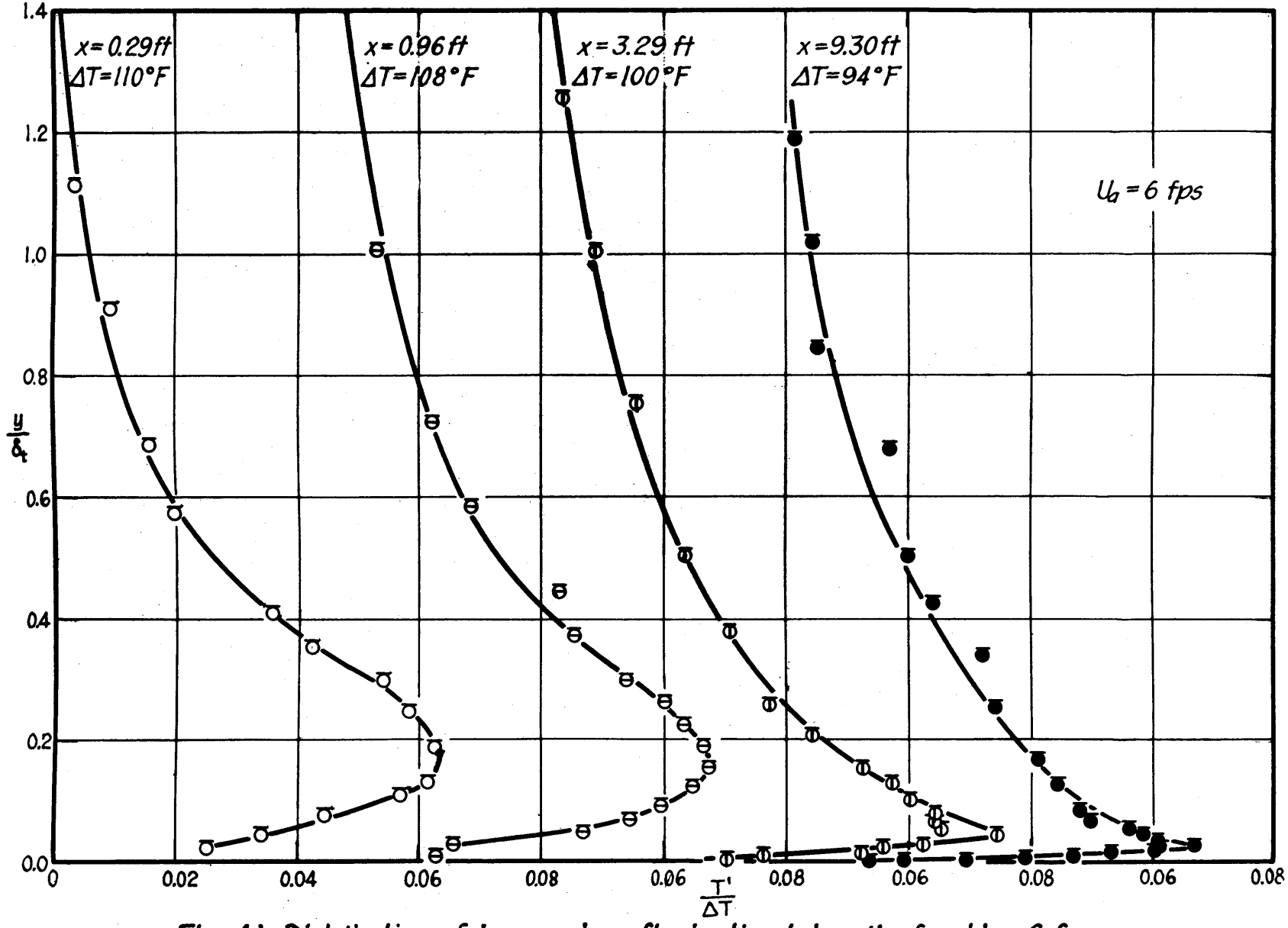

Fig. 41 Distribution of temperature fluctuation intensity for U_a = 6 fps